Beyond trees: Mapping total aboveground biomass density in the Brazilian savanna using high-density UAV-lidar data

Costa, Máira Beatriz Teixeira da; Silva, Carlos Alberto; Broadbent, Eben North; Leite, Rodrigo Vieira; Mohan, Midhun; Liesenberg, Veraldo; Stoddart, Jaz; Amaral, Cibele Hummel do; Almeida, Danilo Roberti Alves de; Silva, Anne Laura da; Goya, Lucas Ruggeri Ré Y.; Cordeiro, Victor Almeida; Rex, Franciel; Hirsch, Andre; Marcatti, Gustavo Eduardo; Cardil, Adrian; Mendonça, Bruno Araujo Furtado de; Hamamura, Caio; Corte, Ana Paula Dalla; Matricardi, Eraldo Aparecido Trondoli; Hudak, Andrew T.; Zambrano, Angelica Maria Almeyda; Valbuena, Ruben; Faria, Bruno Lopes de; Junior, Celso H.L. Silva; Aragao, Luiz; Ferreira, Manuel Eduardo; Liang, Jingjing; Carvalho, Samuel de Pádua Chaves e; Klauberg, Carine

Forest Ecology and Management

DOI:
10.1016/j.foreco.2021.119155

Published: 01/07/2021

Peer reviewed version

Beyond trees: mapping total aboveground biomass in the Brazilian savanna using high-density UAV-lidar data

Máira Beatriz Teixeira da Costa[1], Carlos Alberto Silva[2,3*], Eben North Broadbent [4], Rodrigo Vieira Leite[5], Midhun Mohan[6], Veraldo Liesenberg[7], Jaz Stoddart[8], Cibele Hummel do Amaral[5], Danilo Roberti Alves de Almeida[9], Anne Laura da Silva[10], Lucas Ruggeri Ré Y Goya[10], Victor Almeida Cordeiro[10], Franciel Rex[11], Andre Hirsch[10], Gustavo Eduardo Marcatti[10], Adrian Cardil[12,13,14], Bruno Araujo Furtado de Mendonça[15], Caio Hamamura[16], Ana Paula Dalla Corte[11], Eraldo Aparecido Trondoli Matricardi[1], Andrew Hudak[17], Angelica Maria Almeyda Zambrano[18], Ruben Valbuena[8], Bruno Lopes de Faria[19,20], Celso H. L. Silva Junior[21], Luiz Aragao[21], Manuel Eduardo Ferreira[22], Jingjing Liang[23], Samuel de Pádua Chaves e Carvalho[24], Carine Klauberg Silva[10]

1 Department of Forestry, University of Brasília, Campus Darcy Ribeiro, Brasilia, Brazil - 70.910-900; mairabeatrizteixeira@hotmail.com; ematricardi@gmail.com

2 School of Forest Resources and Conservation, University of Florida, PO Box 110410 Gainesville, FL 32611, c.silva@ufl.edu

3 Department of Geographical Sciences, University of Maryland, College Park, MD 20740, USA

4 Spatial Ecology and Conservation (SPEC) Lab, School of Forest Resources and Conservation, University of Florida, Gainesville, FL 32611 USA eben@ufl.edu

5 Department of Forest Engineering, Federal University of Viçosa (UFV), Viçosa, MG, Brazil; chamaral@ufv.br, rodrigo.leite@ufv.br

6 Department of Geography, University of California—Berkeley, Berkeley, CA 94709, USA; mid_mohan@berkeley.edu

7 Department of Forest Engineering, College of Agriculture and Veterinary, Santa Catarina State University (UDESC), Lages, SC, Brazil; veraldo.liesenberg@udesc.br

8 School of Natural Sciences, Bangor University, Bangor LL57 2W, UK

9 Department of Forest Sciences, "Luiz de Queiroz" College of Agriculture, University of São Paulo (USP/ESALQ), Piracicaba, SP, Brazil; daniloraa@usp.br

10 Federal University of São João Del Rei – UFSJ, Sete Lagoas, MG, Brazil - 35701-970; carine_klauberg@hotmail.com; annelsilva11@gmail.com, lucasgoya42.lr@gmail.com, victorcordeiro.ufsj@gmail.com

11 Department of Forest Engineering, Federal University of Paraná (UFPR), Curitiba, PR, Brazil; anacorte@ufpr.br, francielrexx@gmail.com

12 Technosylva Inc, La Jolla, CA, USA

13 Department of Crop and Forest Sciences, University of Lleida, Lleida, Spain

14 Joint Research Unit CTFC - AGROTECNIO, Solsona, Spain

15 Departamento de Silvicultura, Universidade Federal Rural do Rio de Janeiro, Rua da Floresta, Seropédica, RJ, 23897-005, Brazil; brunomendonca@ufrrj.br

16 Federal Institute of Education, Science and Technology of São Paulo, SP, 11533-160, Brazil; hamamura.caio@ifsp.edu.br

17 US Department of Agriculture, Forest Service, Rocky Mountain Research Station, 1221 South Main Street, Moscow, ID 83843, USA

18 Spatial Ecology and Conservation (SPEC) Lab, Center for Latin American Studies, University of Florida, Gainesville, FL 32611 USA aalmeyda@ufl.edu

19 Federal Institute of Technology North of Minas Gerais (IFNMG), 39100-000, Diamantina, MG, Brazil bruno.lopes@ifnmg.edu.br

20 Department of Forest Science, Federal University of Vales do Jequitinhonha e Mucuri, (UFVJM) Campus JK, Diamantina, MG, Brazil
21 National Institute for Space Research, Earth Observation and Geoinformatics Division,, Av. dos Astronautas, 1758, São José dos Campos SP 12227-010, Brazil
22 Image Processing and GIS Lab (LAPIG), Universidade Federal de Goiás, 74001-970, Goiânia-GO, Brazil
23 Department of Forestry and Natural Resources, Purdue University, West Lafayette, IN, USA
24 College of Forestry, Federal University of Mato Grosso, Av. Fernando Correa da Costa, 2367, Boa Esperança, Cuiabá, MT 78060-900, Brazil
*Corresponding author: Tel: +55(31) 99663- 0407; Email: carlos_engflorestal@outlook.com

Abstract: Tropical savanna ecosystems play a major role in the seasonality of the global carbon cycle. However, their ability to store and sequester carbon is uncertain due to combined, interacting effects of anthropogenic activities and climate change that impact wildfire regimes and vegetation dynamics. Accurate measurements of tropical savanna vegetation aboveground biomass (AGB) over broad spatial scales are crucial to achieve effective carbon emission mitigation strategies. UAV-lidar is a new remote sensing technology that can enable rapid 3-D mapping of structure and related AGB in tropical savanna ecosystems. This study aimed to assess the capability of high-density UAV-lidar to estimate and map total (tree, shrubs, and surface layers) aboveground biomass (AGBt) in the Brazilian Savanna (Cerrado). Five ordinary least square regression models estimating AGBt were adjusted using a sample of 50 field plots (30x30 m^2). The best model was selected under Akaike Information Criterion, absolute and relative root mean square error (RMSE), and the adjusted coefficient of determination (adj.R^2), and used to map AGBt over 1,854 ha UAV-lidar data spanning across the three major vegetation formations (forest, savanna, and grassland). The model using vegetation height and cover was the most effective, with an overall model adj-R^2 of 0.79 and a leave-one-out cross-validated RMSE of 19.11 Mg/ha (33.40%). The uncertainty of our estimations was assessed for each vegetation formation separately, resulting in RMSEs of 27.08 Mg/ha (25.99%) for forests, 17.76 Mg/ha (43.96%) for savannas, and 7.72 Mg/ha (44.92%) for grasslands. These results prove the feasibility and potential of the UAV-lidar technology in Cerrado but also emphasize the need for further developing the estimation of biomass in grasslands, of very high importance in the characterization of the global carbon balance and for supporting integrated fire management activities in tropical savanna ecosystems. Our results serve as a benchmark for future studies aiming to generate accurate biomass maps and provide baseline data for efficient management of fire and predicted climate change impacts on tropical savanna ecosystems.

Keywords: biomass, vegetation, tropical savanna, remote sensing, Cerrado, mapping, GatorEye

Highlights

- UAV-lidar collects data sensitive to vegetation structure in tropical savanna.

- First study to map total aboveground biomass (AGBt) from UAV-lidar in Cerrado.

- Besides tree biomass, AGBt includes surface vegetation layers and shrubs.

- Canopy height and cover were the most effective UAV-lidar metrics to map AGBt in Cerrado.

- AGBt uncertainty was lower in forest and savanna than in grassland formations.

- The study is a step forward in using UAV-lidar for AGBt mapping in tropical savanna ecosystems.

1. Introduction

Tropical savanna ecosystems occupy approximately 20% of the Earth's terrestrial surface and are recognized globally for their species richness and endemic biodiversity (Simon et al., 2009). These ecosystems, characterized by a gradient of vegetation formations ranging from grasslands, savannas, and forests. Wildfires are an important element of the tropical savanna, but natural fire regimes have been altered by anthropogenic activities and climate change (Pivello, 2011; Reichstein et al., 2013). Tropical savannas play a major role in the global carbon budget (Poulter et al., 2014), but their ability to store and sequester carbon, and the combined impacts of their fire regimes and vegetation dynamics on the global carbon balances are still largely unknown (van der Werf et al., 2010; Pugh et al. 2019; Duvert et al., 2020; Lasslop et al., 2020).

The Brazilian Savanna, known as Cerrado, is the second-largest habitat type in South America, after the Amazon biome, spanning two million km^2 (23.3% of the Brazilian territory) (Silva and Bates, 2002; Bonanomi et al., 2019). Cerrado is considered a hotspot for biodiversity and plays an important role in mitigating climate change and global warming by storing carbon from local biomass (Ribeiro et al., 2011). However, Cerrado is severely threatened by increased anthropogenic activities and human-driven changes in fire regime (Durigan and Ratter, 2016). Between 2002 and 2010, the 545,000 km^2 area burned in the Cerrado represented approximately 73% of the total burned area in Brazil (Araújo et al., 2012). Hence, fire strongly shapes the vegetation and ecotones in savannas (Hirota et al. 2011; Staver et al. 2011). By changing vegetation structure, fires also can induce cascading effects that alter habitat quality for fauna (Lindenmayer et al., 2008).

Almost half of the Cerrado has been lost in the last few decades (Souza et al., 2020), and the remaining areas face continuous environmental threats as a result of the expansion of agricultural production to supply the increasing global food demand. Innovative monitoring strategies for understanding the landscape configuration of biomass stocks and their changes are needed in the Cerrado to develop accurate predictive vegetation dynamics and climate models that could support decisions and inform policymakers to define strategies of carbon markets and REDD+ initiatives globally. Moreover, these strategies are crucial to improve forest fire management techniques that could contribute to maintaining ecological values in tropical savannas (Ribeiro et al., 2011; Franke et al., 2018; Levick et al., 2018; Durigan et al., 2020). Given the large latitudinal gradient and the high environmental, structural, and inter and intraspecies variability within the Cerrado biome, data collection requires time and labor-intensive fieldworks (Ottmar et al., 2001; Gwenzi and Lefsky, 2016; Roitman et al., 2018). Although field data provide the most accurate and straightforward estimates, field data collections are constrained by time, financial cost, and labor, making them impractical and expensive to apply for large-scale and/or recurrent studies (Mohan et al., 2017; Goldbergs et al., 2018; Silva et al., 2020). Additionally, direct biomass estimation requires destructive sampling that causes some impacts on local habitat and ecosystem. Integration of mathematical models and indirect measurements using remotely sensed data provide complementary or alternative approaches to estimate biomass and other physical variables (Qureshi et al., 2012; Ribeiro et al., 2017).

Among the remote sensing technologies available, light detection and ranging (lidar) has gained prominence in the last decades due to its ability to provide detailed and accurate characterizations of vegetation vertical structure in tropical savanna ecosystems (Gwenzi and Lefsky, 2016; Levick et al., 2018; Goldbergs et al., 2018; Zimbres et al., 2020). These three-dimensional structural assessments can be undertaken by spaceborne (SLS), airborne (ALS), or terrestrial laser scanning (TLS) platforms, although the latter is constrained by limited spatial footprints and thus is not directly applicable for broad-scale studies (Ferreira et al., 2012; Ribeiro et al., 2017; Silva et al., 2018; Luck et al., 2020; Valbuena et al., 2020; Zimbres et al., 2020; Singh et al., 2021). The advent of unmanned aerial vehicles (UAVs) have further expanded the capabilities of airborne lidar, as UAV-lidar is an easily implementable and cost-effective solution that bridges the scale gap between ALS and TLS collections and improves the accuracy of outputs such as tree height, leaf area density, and biomass (Wang et al., 2019; Almeida et al., 2020; Dalla Corte et al., 2020; Harkel et al., 2020; Shendryk et al., 2020).

Notwithstanding the demonstrated potential of lidar in estimating biomass at both landscape and regional scales by previous studies (Drake et al., 2002; Naesset and Gobakken, 2008; Hudak et al., 2020), they are still rarely implemented in tropical savanna. Additionally, the majority of the undertaken studies have placed their primary focus solely on the estimation of biomass from trees, using ALS and TLS (e.g., Bispo et al. 2020; Zimbres et al., 2020), or the recent SLS missions, such as NASA Global Ecosystem Dynamics Investigation (GEDI) (Dubayah et al. 2020; Marselis et al. 2019; Marselis et al. 2020). The very few studies that have ventured into estimating individual biomass components have limited their purview with the assessment of biomass contributions from tree strata, such as leaves, branches, and stems (García et al. 2010; Silva et al. 2014; Hernando et al. 2017; Scaranello et al. 2019). However, a significant portion of the total aboveground biomass in tropical savanna is composed of surface biomass (duff, litter, downed woody material, shrub, and herbaceous), which are not taken into account by the foregoing studies. These, however, have great influence on fire regimes and associated carbon cycles (Pivello, 2011). Therefore, it is crucial to fill in the gap between global carbon fluxes and current remote sensing estimations of biomass in terrestrial ecosystems, with the development of models that account for large components of ecosystem biomass that remain unaccounted for when only woody tree biomass is considered (Dass et al., 2018).

Even though lidar has proved to be beneficial for capturing the 3-D structures of the vegetation in savanna ecosystems (Anderson et al., 2018; Bispo et al. 2020; Zimbres et al., 2020), there is a need to develop a framework for mapping total (woody, shrubs and surface vegetation) aboveground biomass (AGBt) and evaluate the applicability of UAV-lidar for AGBt in tropical savanna ecosystems. This study aimed to assess the capability of high-density UAV-lidar to estimate and map AGBt across the structurally complex vegetation formations of the Cerrado in Brazil. Herein, we developed a framework for: (i) selecting the best UAV-lidar metrics to build AGBt models; (ii) shortlisting the best models to predict AGBt; (iii) estimating AGBt at plot level; and (iv) mapping AGBt at the landscape level, assessing its spatial distribution and uncertainty across the main Cerrado vegetation formations: grassland, savanna, and forest. Given the resource-grade accuracy available through high-density UAV-lidar (Wilkinson et al., 2019), we hypothesize that it would be possible to map AGBt in Cerrado at a satisfactory precision, and we expect to identify biome-specific technological challenges that need to be addressed for furthering our understanding of the existing ecosystem intricacies and advancement of carbon management paradigms. Since there exist no other UAV lidar-based studies on total AGB estimates for the Cerrado biome, this work is intended to serve as a benchmark for future studies and should help generate consistent AGBt maps with changing climate and environment.

2. Material and Methods

2.1. Study area

Our study sites are located at the Serra do Cipó National Park (SCNPK), Chapada dos Veadeiros National Park (CVNPK), Paraopeba National Forest (PNF), and University of São João Del-Rei's Forest (UFSJ) (Figure 1).

SCNPK (19°12'-34'S, 43°27'-38'W) is located in the southeast portion of the Cerrado biome, state of Minas Gerais. The region's climate is mesothermal, Cwb (subtropical of altitude) according to Koppen's classification (Alvares et al., 2013), with dry winters and rainy summers, and the annual average of cumulative rainfall is ca. 1,400 mm, with a rainy season occurring between October and March, and monthly rainfall ranging from 75 to 340 mm (Alvarado et al., 2017). The average annual temperature ranges 17.0°-18.5°C. The study site's topography is rugged and predominantly mountainous, with elevations ranging from 750 to 1,670 m above sea level (a.s.l.) (Ribeiro and Figueira, 2017). The vegetation in SCNPK varies and comprises different physiognomies, from open grasslands ("Campo Limpo") at altitudes below 1,000 m to savanna formations with different proportions of woody cover ("Campo Sujo", "Campo Cerrado" and "Cerrado sensu stricto") and forest formations ("Cerradão"), all classified as part of the Cerrado sensu lato (Oliveira-Filho and Ratter, 2002); above 1,000 m are found the rupestrian grasslands (Benites et al., 2003). The soils are diverse and vary according to the vegetation formations, being greatly determined by local topography and microenvironmental aspects; in savanna and forest formations, there are latosols and cambisols, while in the rupestrian grasslands there are litholic neosols and spodosols (Schaefer et al., 2016).

The CVNPK (13°51'-14°10'S, 47°25'-42'W) encompasses five municipalities in the state of Goiás, Brazil. Within a mountainous region, the altitude in CVNPK ranges from 620 to 1,700 m a.s.l., and the climate is characterized as tropical and sub-humid (AW) (Alvares et al., 2013). The average temperatures range from 20° to and 26°C (Silva et al., 2001). The landscape is formed by mosaics of different vegetation types (Ribeiro and Walter, 2008) characterized by a predominance of forest formations at low elevations and Cerrado with montane savannas at high elevations (Felfili et al. 2007). Wet and dry grasslands and savannas occur in between streams, covering most of the landscape. At the northwest edge of the park, dry deciduous forests are found, whereas at the southwest edge riparian evergreen forests are most common (Flores et al., 2020). In total, the CVNPK presents 77% of savanna formation, and about 10% corresponds to the forest fragments (Porto et al., 2011). Cambisols and litholic neosols occupy the largest area of the park (IBAMA, 1998).

The PNF (19° 20'S and 44° 20'W) is located in the municipality of Paraopeba, state of Minas Gerais, Brazil. It is comprised of 150 ha remnants of Cerrado vegetation, including both savanna (e.g. Cerrado *sensu stricto*) and forest formations (e.g.Cerradão) (Neri et al., 2013). The altitude in PNF ranges from 734 to 750 m a.s.l., and the climate is characterized by the humid subtropical type (Cfa) (Alvares et al. 2013), with a rainy summer from January to March and a dry season that varies from April to September, reaching a mean annual precipitation of 1,236 mm (Balduino et al. 2005). The soils range from Latosols (red, red-yellow, and yellow) to Cambisols and Fluvic Neosols (Neri et al., 2013).

The UFSJ forest (19°28'S, 44°11'W) is located in the Sete Lagoas municipality, state of Minas Gerais, Brazil, at an altitude a.s.l. that ranges from 742 to 815 m . The local climate is considered tropical altitude (Cwa) (Alvares et al., 2013), with a well-defined dry winter and rainy summer. The average annual temperature is 21.73°C, and the mean annual precipitation is 1,330 mm (Guimarães and Rios, 2010). The predominant vegetation type is Cerrado *sensu stricto* characterized by the dominance of trees with scattered shrubs and grass understorey. The climate is of the humid subtropical type, with a dry winter and moderately hot summer (Alvares et al., 2013). The soils are predominantly Oxisols (red latosol and red-yellow Latosols).

Altogether, our four study sites comprise various Cerrado vegetation physiognomies that represent a wide range in vertical and horizontal structures, and also in species diversity and provenances. Herein, we classified the vegetation of our study sites into three major formations according to Ribeiro and Walter (2008) and defined as: (i) grasslands, mostly represented by a shrub-herbaceous layer with absence or randomly sparse higher shrub individuals; (ii) savannas, which stands out by one shrub-herbaceous layer and one tree layer well defined, where the latter layer density ranges and never closes completely; and (iii) forests, mostly represented by a continuous tree layer but also very structurally diverse as a result of the species communities partitioning under different environmental conditions. (Fig. 2).

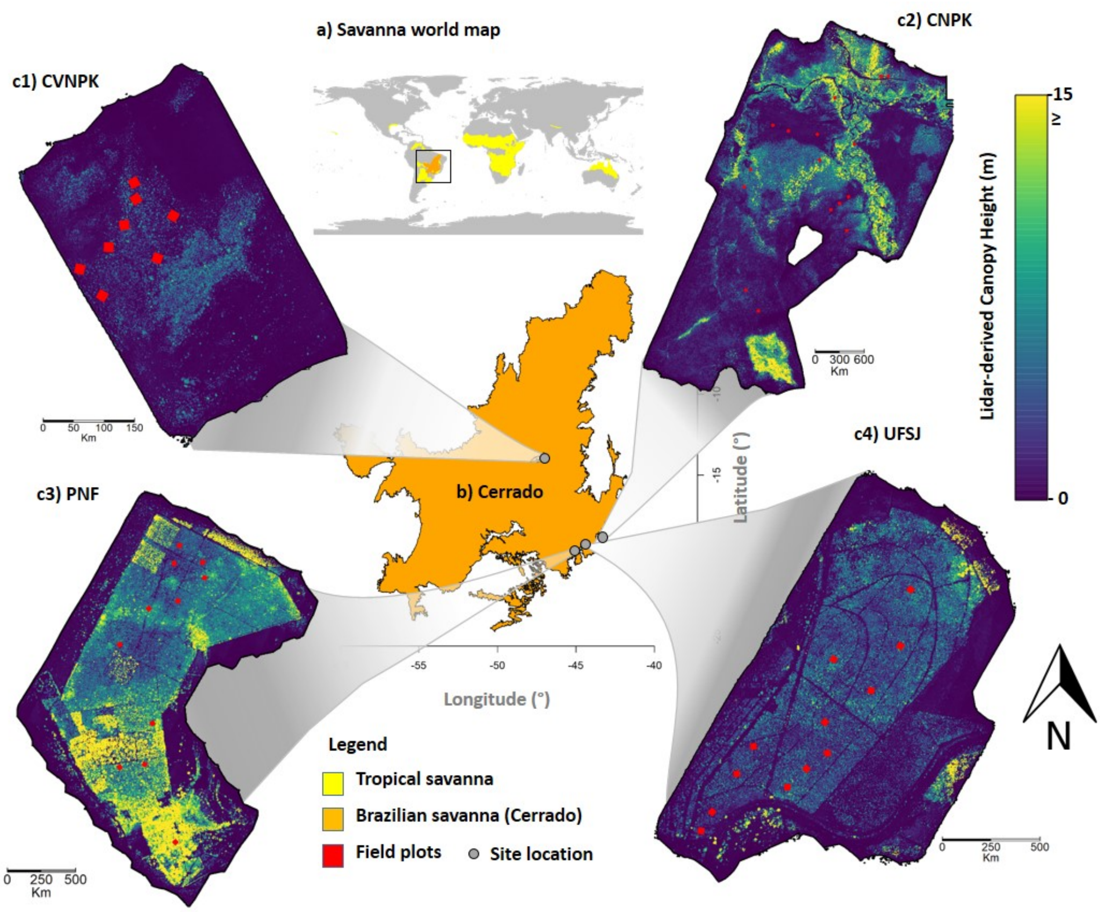

Figure 1. Map of the UAV-lidar-derived canopy height model within the study area in the Brazilian Savanna. Serra do Cipó National Park (SCNPK), Chapada dos Veadeiros National Park (CVNPK), Paraopeba National Forest (PNF), and University of São João Del-Rei's Forest (UFSJ).

2.2. Field measurements

Field plots of 30×30 m (900 m²) covering all the Cerrado formations (Fig. 2) were established between June and July of 2019 for measuring the vegetation total aboveground biomass (AGBt). Plot corners were registered using a Differential Global Navigation Satellite System (DGNSS). The aboveground biomass of trees

(AGB_{Trees}, in Mg/ha) was determined from measurements of all individual trees within the plot with a diameter at breast height (dbh, in cm) ≥ 10 cm. Every tree was taxonomically identified, and their heights (ht, in m) and dbh were measured using a clinometer and diameter tape, respectively. Within each plot, two 2×5 m sub-plots were established to determine the aboveground biomass of shrubs and small trees (dbh < 10 cm) (AGB_{ST}, in Mg/ha). For each plot, four 1×1 m sub-plots were established for determining the aboveground biomass of surface vegetation (AGB_{SB}, in Mg/ha). The AGBt was derived from the total sum of biomass (in kg) measured within each plot and sub-plots and then transformed into total biomass densities (in Mg/ha) using their corresponding hectare expansion factors (HEF).

Individual tree dry biomass was estimated in the field using a published allometry equation calibrated (Eq. 1) based on dbh, ht and wood density (ϱ) information (Chave et al 2014). Total dry tree biomass (AGB_{ST}, in Mg/ha) was computed by summing up individual tree biomass to the plot level (Eq. 2):

$$AGB_{Tree\_i} = 0.0673 \times (\varrho \times dbh_i^2 \times ht_i)^{0.976} \quad \text{(Eq.1)}$$

$$AGB_{Trees} = \sum_{i=1}^{n} AGB_{tree_i} \times HEF_{Trees} \quad \text{(Eq.2)}$$

where: dbh is in cm, ht is in m, and ϱ is in $g.cm^{-3}$. AGB_{Trees} represents the total dry tree biomass at the plot level, AGB_{Tree_i} represents dry biomass per tree i, and n represents the number of trees for each plot i, and HEF_{Trees} = 11.11. Wood density values ϱ were derived from Zanne et al. (2009).

For measuring the AGB stock in the 2×5 m shrub sub-plots, we harvested all the shrubs and small trees and weighed them using a 10 g precision scale. Three ~500 g samples per sub-plot containing both the shrub and tree components (stems, branches, and leaves) were sent to the laboratory to measure the weights of wet biomass (WB, in g) and dry biomass (DB, in g) biomass. Average WB and DB values were used to calculate moisture content (MC_i, in %) for each sub-plot, according to Eq. 3. Total dry shrub and small tree (AGB_{ST}, in Mg/ha) was then calculated as:

$$MC_i = \frac{WBi - DBi}{WBi} \quad \text{(Eq.3)}$$

$$AGB_{ST} = \sum_{i=1}^{n} AGB_{ST_i} \times HEF_{ST} \times (1-MC_i) \quad \text{(Eq.4)}$$

where AGB_{ST} is the dry shrub and small tree biomass at the plot level, AGB_{SBi} is the wet shrub and small tree biomass for sub-plot i (in kg), MC_i is the moisture content calculated for each sub-plot, and HEF_{ST} = 500.

For computing the surface vegetation biomass at the plot level, in the field, we collected and weighed the biomass in the duff, litter, downed woody material, and herbaceous material found within the 1×1 m sub-plots. Again, three ~500 g samples per sub-plot were also collected and sent to the laboratory for computing the MC_i for the surface biomass (Eq. 3). The total dry surface biomass (AGB_{SB}, in Mg/ha) was then calculated as:

$$AGB_{SB} = \sum_{i=1}^{n} AGB_{SB_i} \times HEF_{SB} \times (1-MC_i) \quad \text{(Eq. 5)}$$

where AGB_{SB} is the dry surface biomass at the plot level, and AGB_{SBi} is the wet surface biomass for sub-plot i (in kg), MC_i is the moisture content calculated for each sub-plot, and HEF_{SB} = 2,500.

Finally, the total dry aboveground biomass (AGBt, in Mg/ha) at the plot level was then computed by summing the AGB_{tree}, AGB_{ST}, and AGB_{SB} measurements (Eq. 6).

$$AGBt = AGB_{Trees} + AGB_{ST} + AGB_{SB} \quad \text{(Eq.6)}$$

The summary of AGBt within all the field plots and stratified by Cerrado formations is presented in Table 1.

Table 1. Summary of the total aboveground biomass (AGBt) within our field plots and stratified by Cerrado formations.

Cerrado formation	Number of plots	AGBt (Mg/ha)			
		min	max	mean	sd
Grassland	5	11.65	25.86	17.19	7.30
Savanna	30	13.32	100.22	40.39	23.55
Forest	15	43.68	187.94	104.21	42.39

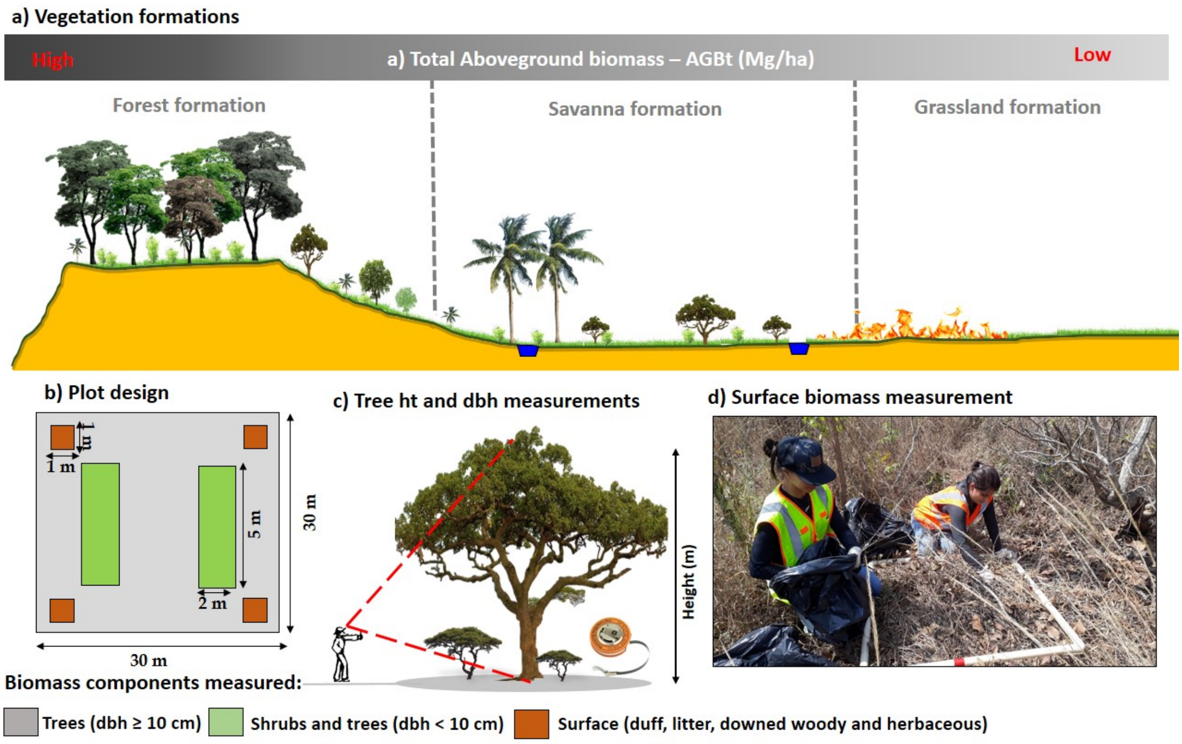

Figure 2. Illustration of field data collection. a) Cerrado formation, b) design of field plots and subplots for measuring the total aboveground biomass (AGBt), and c) Tree dbh and height measurements, d) surface biomass measurement.

2.3. UAV-lidar

Our study sites were scanned using the GatorEye UAV-lidar system (Fig. 3) (Almeida et al., 2020; Prata et al., 2020; Dalla Corte et al., 2020) during two weeks in July 2019, which was nearly simultaneous with the field data collection. The GatorEye uses a DJI M600 Pro planform mounted with a Phoenix Scout Ultra core to integrate lidar with an inertial motion unit (Novatel STIM 300), and cm accuracy differential GNSS system, which have a combined weight of approximately 4.5 kg. The lidar sensor, which was uniquely used in this study, was a Velodyne VLP-32c dual-return laser scanner which has a total of 32 separate lasers each having a 360° vertical field of view (FOV) and which are distributed to permit an instantaneous 40° along-track FOV. The laser suite emitsa total of 600,000 pulses per second and a theoretical return number of 1,200,000 per second, which during flight with an across-track FOV of 120° creates a realized approximate 350,000 returns per second, with the remaining going out of range. A ground base station X900S-OPUS GNSS receiver collected static GNSS data, which were used to calculate a PPK (post-processed kinematic) flight trajectory using Novatel Inertial Explorer software. Absolute point accuracy was tested using ground-surveyed DGNSS checkpoints, and it was accepted when showing a root mean square error (RMSE; eq. 10) below 5 cm (Wilkinson et al., 2019). Detailed information and data downloads can be found at the GatorEye website (www.gatoreye.org) (Broadbent et al., 2020) and in d'Oliveira et al. (2020). The autonomous flight was programmed to survey at a mean speed of 14 m/s at around 100 m above ground level (a.g.l.), with flightlines spaced 100 m apart. In total, across the four study sites, we flew approximately 600 km of flight lines covering 1,854 hectares, which to our knowledge is the largest area of UAV-lidar used in a publication (as of 12/16/20). The final merged point clouds were about 100 GB in total size and had a very high-density of approximately 450 points/m^2 across all study sites.

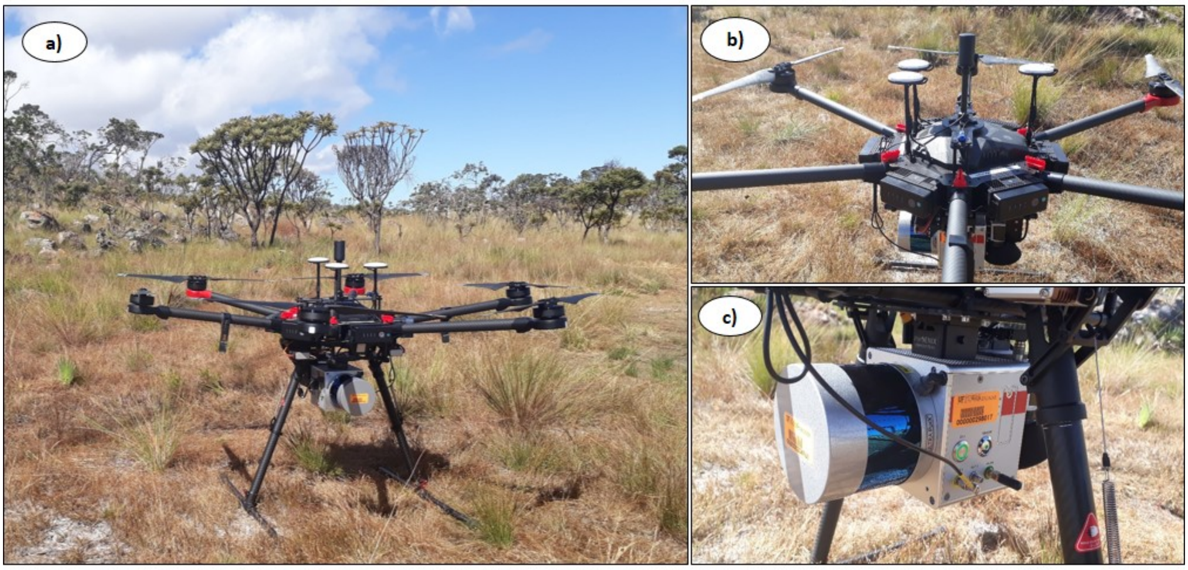

Figure 3. GatorEye UAV-lidar system. a) GatorEye UFL (Gen 1) system, with Phoenix Scout Ultra, hyperspectral, and visual sensors on a DJI M600 Pro airframe; b) GNSS antennas for navigation (three) and sensor trajectory (middle); and c) Velodyne Ultra Puck (lidar system).

The UAV-lidar 3-D point cloud data was processed using the GatorEye Multi-scalar Post-Processing Workflow, followed by further flight line alignment using Bayes StripAlign software, as it is described in detail in Broadbent et al. (2020). The final elliptical merged point clouds were further processed using Lastools (Isenburg, 2020). First, the las files were divided into tiles of 200 m for ground returns classification via *lasground* (spike: 1 m, bulge: 0.5 m, step: 10 m, offset: 0.05 m). Digital terrain models (DTM) were created with a spatial resolution of 1 m via the *blast2dem* and used for normalizing the 3-D point cloud to height a.g.l.via *lasheight*. The *Lasclip* tool was used for clipping the point cloud within the field plots, and the *lascanopy* tool was applied for computing a suite of lidar metrics per plot and for the entire lidar coverage as grid layers with a spatial resolution of 30 m (see Table 2).

Table 2. UAV-lidar derived metrics.

Class	Metrics	Description
Height	HMEAN	Height mean
	HMAX	Height maximum
	HSD	Height standard deviation
	HKUR	Height kurtosis
	HSKE	Height skewness
	HOME	Height of Median Energy
	H25TH	Height 25th percentile
	H50TH	Height 50th percentile
	H70TH	Height 70th percentile
	H75TH	Height 75th percentile
	H80TH	Height 80th percentile
	H85TH	Height 85th percentile
	H90TH	Height 90th percentile
	H95TH	Height 95th percentile

	H98TH	Height 98th percentile
	H99TH	Height 99th percentile
cover	COV	cover

2.4. Modeling development and assessment

Our modeling framework was based on linear regression models (Eq. 7) fitted using the ordinary least squares (OLS) estimator (Eq. 8). Herein, a family of five models was developed in two steps by first removing high correlated metrics, and second selecting the best models using the subsets of predictors (Hudak et al., 2006; Silva et al., 2014). First, Pearson's correlation (r) was used to identify and exclude highly correlated variables using a ±0.9 threshold. Subsequently, we applied an exhaustive variable selection algorithm to find the best linear models with up to six predictors using the *regsubsets* function of the R package leaps (Hudak et al., 2006; Lumley, 2020). The linear models were fitted using the natural logarithm transformation of the AGBt as a response and the non-correlated lidar-derived metrics as predictor variables. The heteroscedasticity and normality of the model residuals were tested with the Breusch-Pagan (Breusch and Pagan, 1979) and Shapiro-Wilk (Shapiro and Wilk, 1965) tests at the significance level of 0.05.

$$Y_S = X_S\beta + \varepsilon_S \quad \text{(Eq. 7)}$$

where: Y_S is the n-length column vector of the response variable AGBt in sample S; X_S is an n x (p + 1) matrix of the lidar metrics used as predictors and a unit vector as the first column; β is a column vector of model parameters of length (p + 1); and ε_S is the n-length column vector of random errors with E(ε_S) = 0 and ε_i~N(0,σ_ε^2). Using the sample S of n = 50 plots, the vector of model parameters was estimated for each model as:

$$\hat{\beta}_S = (X_S^T X_S)^{-1} X_S^T Y_S \quad \text{(Eq. 8)}$$

where: $\hat{\beta}_S$ is a column vector of estimated model intercept and parameters with length (p + 1), and p is the number of predictors.

We calculated the adjusted coefficient of determination (adjR²) and the absolute and relative root mean square error (RMSE and %RMSE, respectively), and absolute and relative mean differences (%MD), between the estimated and observed AGBt values (Eqs. 9-13) to assess the models' performance. The models were ranked using the corrected Akaike information criterion (AICc, Eq. 14) (Sugiura, 1978; Hudak et al., 2006). The AICc can be applied when the number of observations is relatively small (n/p < 40) and computes an additional penalization for the number of parameters to the AIC (Akaike 1979).

$adjR^2 = 1 - \frac{(1-R^2)(n-1)}{n-p-1},$	(Eq. 9)
$RMSE = \sqrt{\frac{\sum_{i=1}^{n} (\hat{Y}_i - Y_i)^2}{n}},$	(Eq. 10)
$\%RMSE = \frac{RMSE}{\underline{Y}} \times 100,$	(Eq. 11)
$MD = \frac{\sum_{i=1}^{n} (\hat{Y}_i - Y_i)}{n},$	(Eq. 12)
$\%MD = \frac{MD}{\underline{Y}} \times 100,$	(Eq. 13)
$AICc = AIC + 2p\frac{(p+1)}{(n-p-1)},$	(Eq. 14)

where: $\hat{Y}_i$ is the estimated AGBt; Y_i is the observed AGBt; $\underline{Y}$ is the sample mean observed AGBt; n is the number of observations, and p is the number of predictors.

All performance assessments were carried out using the AGBt on its original scale. The back-transformation was conducted by applying the inverse natural logarithm to the AGBt values. The estimated values were further multiplied by a correction factor (Eq. 15) to reduce MD related to the log-transformation (Smith 1993, Hudak et al. 2006).

$cf = e^{(0.5 \, x \, MSE)},$	(Eq. 15)

where: MSE is the mean squared error of the residuals.

The model performances were also estimated for the different Cerrado formations (grassland, savanna, and forest). The best-ranked model was further assessed with a leave-one-out cross-validation (LOOCV) and R^2, absolute and relative RMSE and MD were also calculated based on the observed and estimated AGBt values derived from the LOOCV procedure within each vegetation formation. The Wilcoxon–Mann–Whitney rank-sum (W) test (Wilcoxon, 1945) was applied to assess if the estimated and observed AGBt differ at the significance level of 0.05.

2.5. Aboveground biomass mapping

The best linear model was implemented across the entire landscape, to map the AGBt in the study site. In this step, the lidar-derived metrics used as predictors were calculated for a spatially-continuous grid of 30×30 m cells, and the model was applied to every grid cell across all the study sites. The Cerrado formations were delineated based on visual interpretation of high spatial resolution GatorEye UAV RGB and Planet's imagery (Planet Team, 2017), conducted by an experienced local photo-interpreter.

Accounting for the uncertainty of the estimates is important when combining inventory and remote sensing data to map forest attributes (Persson and Stahl, 2020). We accounted for the uncertainty for each Cerrado formation by calculating the variance of the estimator ($V[\widehat{E(\mu)}_i]$) estimated using standard model-based inference (Saarela et al. 2016, Stahl et al. 2016, Puliti et al. 2018). In this approach, the sample S used to develop the models in section 2.4 was considered a draw from a larger population U. The Ui represents the finite population of the i-th Cerrado formation with Ni grid-cells. Considering the OLS-estimated parameters $\hat{\beta}_S$ (Eq. 8), the expected mean value ($\widehat{E(\mu)}_i$) and $V[\widehat{E(\mu)}_i]$ for the i-th Cerrado formation can be estimated with Eq. 16 and Eq. 17.

$$\widehat{E(\mu)}_i = \iota_{Ui}^T X_{Ui} \hat{\beta}_S, \quad \text{(Eq. 16)}$$

where: ι_{Ui} is the Ni-length column vector with values 1/Ni for the Ni grid cells of population Ui of the i-th vegetation type; X_{Ui} is a Ni x (p + 1) matrix of the lidar metrics used as predictors and a unit vector as the first column.

$$V[\widehat{E(\mu)}_i] = \iota_{Ui}^T X_{Ui} Cov(\hat{\beta}_S)\, X_S^T \iota_{Ui}, \quad \text{(Eq. 17)}$$

where: $Cov(\hat{\beta}_S)$ is the covariance matrix of the model parameters $\hat{\beta}_S$. Assuming that the estimated errors are homoscedastic the $Cov(\hat{\beta}_S)$ as calculated by Eq. 18.

$$Cov(\hat{\beta}_S) = \frac{\hat{\varepsilon}_S^T \hat{\varepsilon}_S}{n-p-1} (X_S^T X_S)^{-1}, \quad \text{(Eq. 18)}$$

where: $\hat{\varepsilon}_S$ is the vector of the estimated residuals for the model developed using the sample S (Eq. 16).

The standard error $\widehat{SE}_i$ is subsequently then estimated as the $\sqrt{V[\widehat{E(\mu)}_i]}$ and the $\%\widehat{SE}_i$ as a percentage of the mean estimated AGBt.

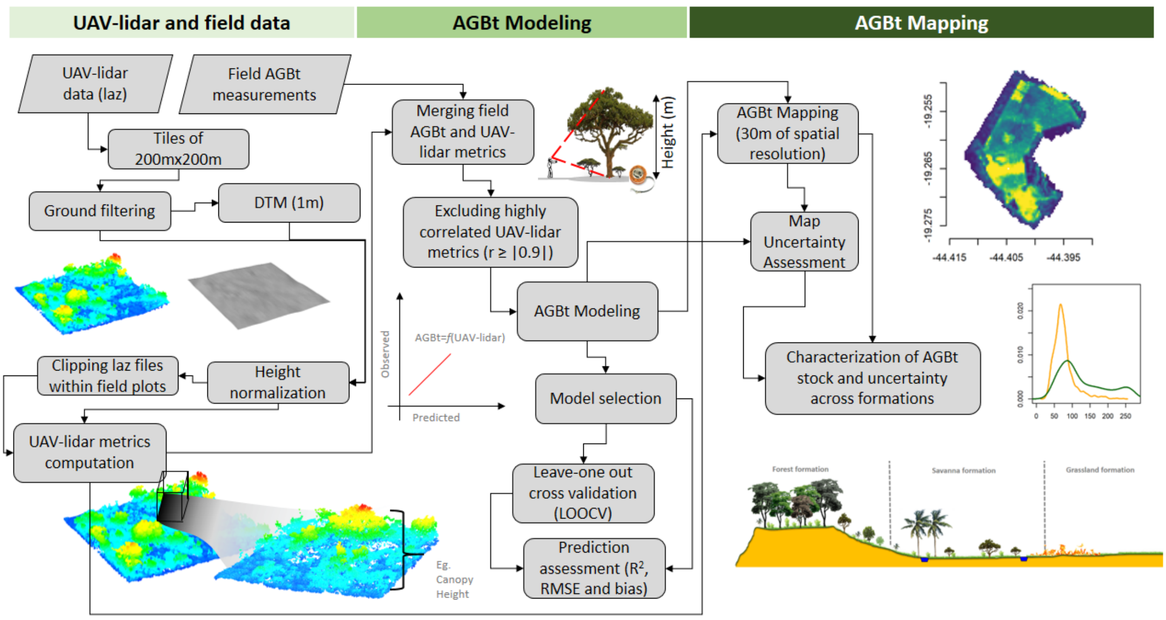

Figure 4. Workflow for the UAV-lidar data processing, AGBt modeling, and mapping.

3. Results

3.1. UAV-lidar metrics

Figure 5 shows the Pearson's correlation test (r) among the 17 UAV lidar-derived metrics (Table 2). In general, 12 metrics were highly correlated ($|r| > 0.9$) with each other under the adopted threshold criteria and were therefore excluded from further analysis (Fig. 5). We kept one of the highly correlated metrics (H98TH) and along with the four-remaining metrics (i.e., COV, H50TH, HKUR, and HSKE) we built the prospective models to estimate AGBt. Three variables were positively correlated, such as H98TH, COV, and H50TH, while two others were negatively correlated, such as HKUR, and HSKE (Fig. 4). Although the number of metrics was reduced to five, the above mentioned lidar-derived metrics still represented important attributes of the vegetation, such as the dominant height (e.g., H98TH), the canopy coverage (e.g., COV), and the vegetation's height asymmetry (e.g., HSKE).

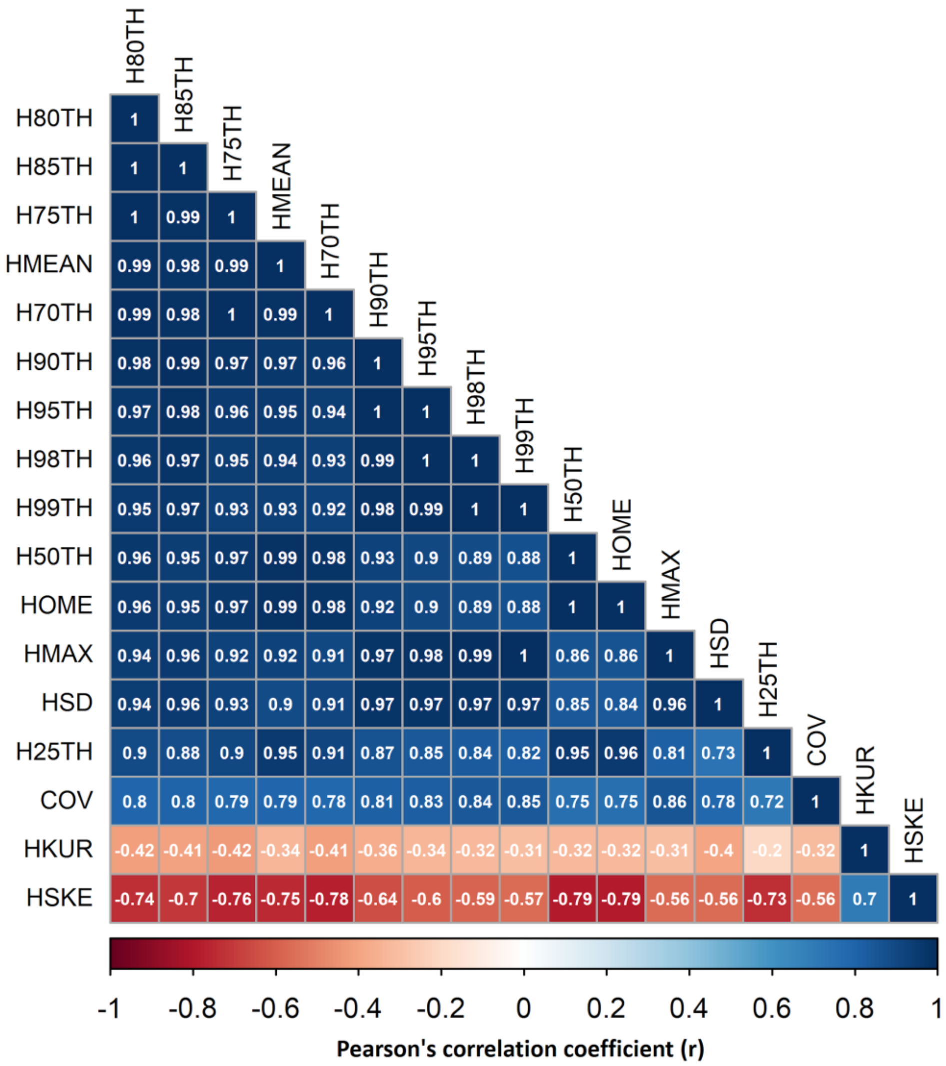

Figure 5. Pearson's correlation (r) diagram among the 17 lidar-derived metrics using a $|r| > 0.9$ threshold. The values are ranked using a color gradient from -1 to 1, where 0 means no correlation and 1 a strong correlation. The negative and positive signs indicate inverse and direct relationships between two variables, respectively.

In grasslands, the lidar returns were more concentrated near the ground (Fig. 6.a1-a3) because of the lower vegetation structure and variability found in this formation. This is clearly illustrated by inspecting the 3-D view perspective of the lidar point cloud for the formation types in Cerrado (Fig. 6.a1-a3). The grasslands observed in the four selected study areas were usually found and arranged in small patches among both forests and savannas. Grasslands showed a predominantly regular height distribution over the landscape and showed a very high density of herbaceous plants per unit area, which makes lidar returns' penetration difficult. In savanna formations, UAV-lidar vegetation height exceeded 10 m and showed higher structural variability than grasslands (Fig. 6.b1- 6.c1). The lidar height returns were sparsely and randomly distributed within shrubs and isolated trees (Figure 6.b3). In forests, the lidar height returns were more distributed in the lowest and topmost height strata showing two to three well-defined canopy strata (Figure 6.c3).

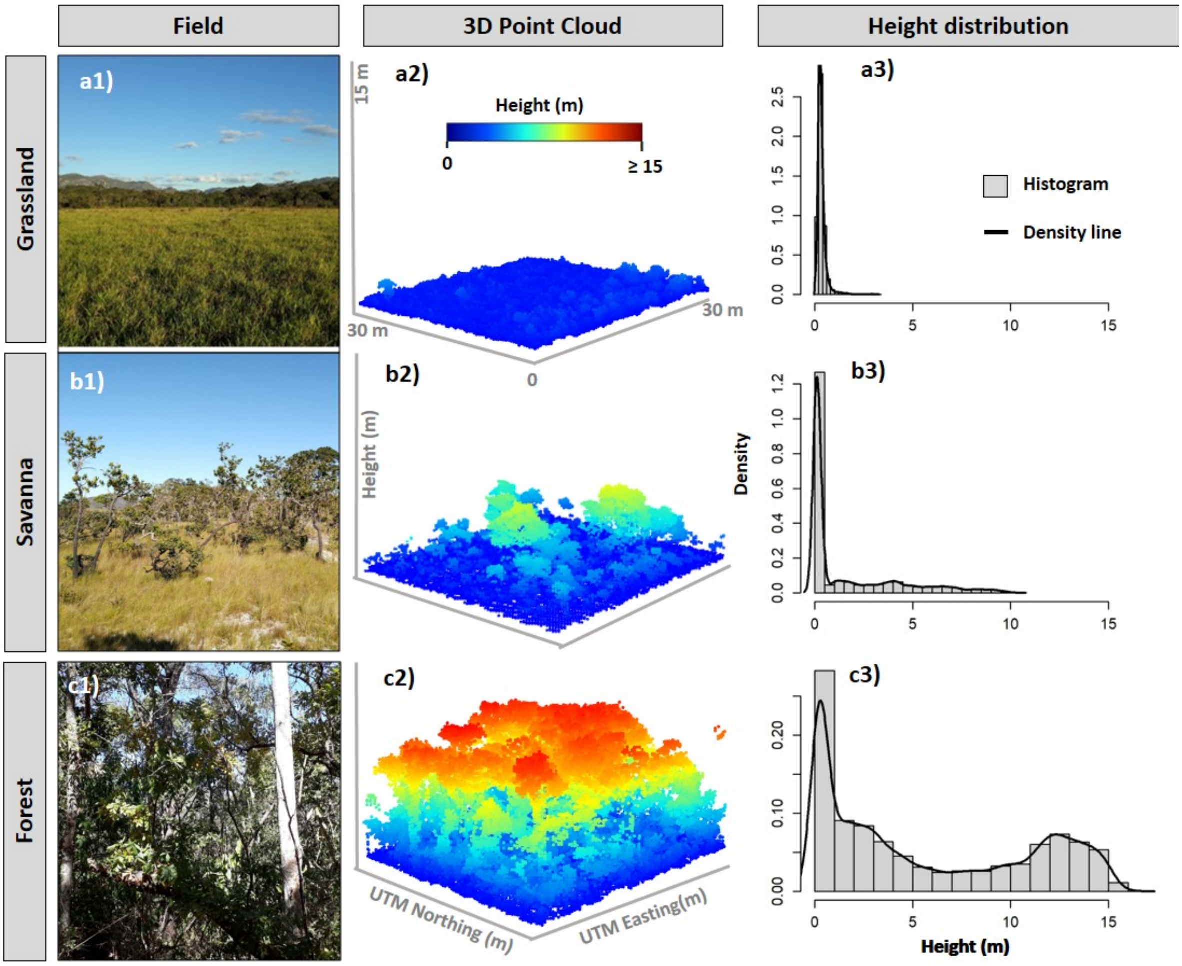

Figure 6. Ground pictures were taken during the field measurements (a-c1). 3-D point cloud perspectives for selected sample plots surveyed by UAV-lidar and where different biophysical properties were measured (a-c2). Density plots of lidar height returns for the three major formations (a-c3). The letter indicates the vegetation formation and is identified in order as grassland (starting with the letter a), savanna (starting with letter b), and forest (starting with letter c).

3.2. Model performance assessment

Table 3 shows five models tested in this study based on the use of the five selected lidar metrics (H98TH, COV, H50TH, HKUR, and HSKE). The first model contains only the metric H98TH, while for the other models we increased the number of variables by adding the remaining lidar metrics, only one per model, based on the exhaustive variable selection approach.

The most suitable model for estimating AGBt showed H98TH and COV only, as they were the best predictors among the suite of lidar metrics (Table 3). This model produced the lowest AICc and satisfied residual normality and homoscedasticity assumptions based on the Shapiro–Wilk (W = 0.95 and p-value = 0.07) and Breusch–Pagan (BP > 1.47 and p-value > 0.48) tests.

Table 3. Comparison of calibrated models using UAV-lidar derived metrics for estimating total aboveground biomass (AGBt) in Cerrado. The description of the UAV-lidar-derived metrics is shown in Table 2.

Predictors	**adjR²**	**RMSE (Mg/ha)**	**RMSE (%)**	**MD(Mg/ha)**	**MD (%)**	**AICc**
H98TH	0.74	24.30	42.46	-1.79	-3.12	44.11
H98TH, COV	0.79	19.11	33.40	-0.26	-0.46	36.49
H98TH, COV, H50TH	0.77	20.25	35.40	-0.70	-1.23	42.59
H98TH, COV, H50TH, HKUR	0.77	19.88	34.75	-0.59	-1.02	51.71
H98TH, COV, H50TH, HKUR, HSKE	0.76	20.14	35.21	-0.60	-1.05	63.13

Note: Adjusted coefficient of determination (Adj R^2), absolute (Mg/ha) and relative (%) root mean square error (RMSE) and mean differences (MD); Akaike's information criterion corrected for a small sample size (AICc).

Fig. 7a shows the performance of the best model using the LOOCV procedure. Fig. 7b shows the distribution of the estimated vs. observed AGBt derived from the LOOCV. Based on the LOOCV results for the best model (Fig. 7a-b), the model slightly underestimated AGBt over lower intervals, and there occurred slight overestimation AGBt in higher intervals. Nevertheless, despite the small differences, the model accuracy as assessed by the LOOCV procedure showed estimates with a MD less than 1 Mg/ha (< 1%), which reveals the robustness of the selected model.

According to the Wilcoxon rank sum test, the AGBt estimates derived from LOOCV did not significantly differ from the observed values (p-value = 0.6918).

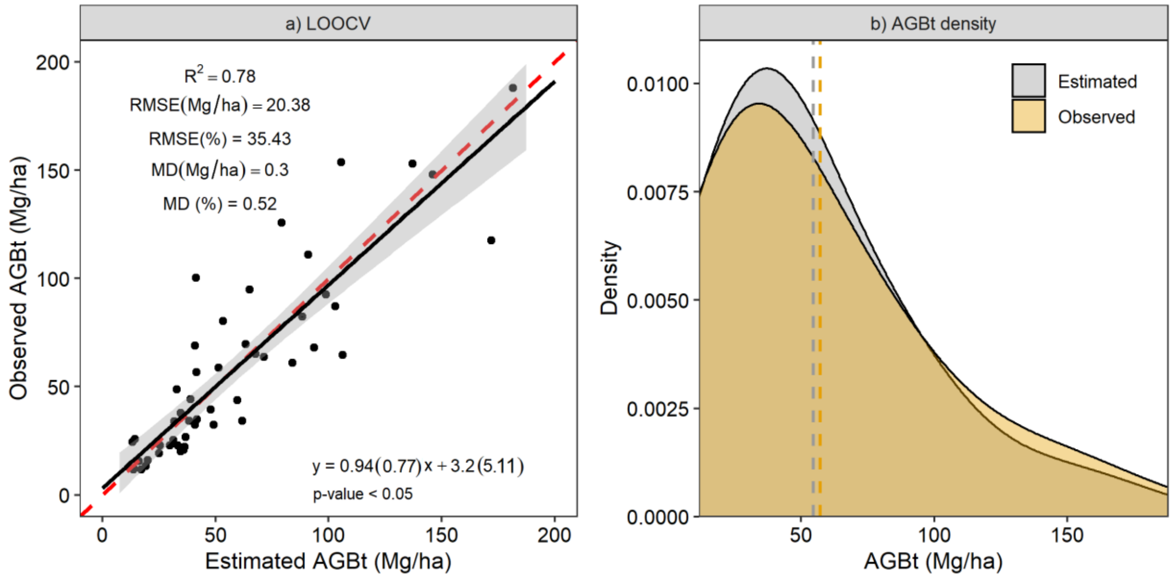

Figure. 7. (a) Scatterplot of cross-validation predictions versus observations (N=50) for the natural-logarithm-transformed total aboveground biomass (AGBt) using the leave-one-out cross-validation (LOOCV). The dashed red line indicates the 1:1 relationship, whereas the black line indicates the best fit. Numbers in parentheses are the standard errors for each coefficient. (b) Frequency distribution of both the estimated and the observed distribution of the AGBt. The dashed line indicates the mean AGBt for both datasets.

Table 4 shows AGBt estimation accuracies from both the calibration and LOOCV procedures by applying the best model summarized by the Cerrado formations. In general, the estimated accuracy of the calibrated model and LOOCV showed similar trends, although as expected cross-validation performed slightly worse based on relative RMSE and MD. Perhaps due to the sample size (n), the grassland model showed the lowest precision (%RMSE) accuracy (%MD) compared to the savanna and forest models. The forest model was most precise (lowest %RMSE) while the savanna model was most accurate (lowest %MD).

Table 4. Summary of absolute and relative RMSE for the calibrated model and LOOCV AGBt predictions stratified by vegetation formations in Cerrado. n= number of observations (field plots) per formation.

Model	**Formation**	**RMSE**	**MD**	**n**

		Mg/ha	%	Mg/ha	%	
Calibration model	**Grassland**	7.16	41.63	2.52	14.65	5
	Savanna	17.24	42.69	-0.17	-0.43	30
	Forest	24.61	23.62	-1.37	-1.32	15
LOOCV	**Grassland**	7.72	44.92	2.71	15.74	5
	Savanna	17.76	43.96	-0.28	-0.68	30
	Forest	27.08	25.99	-1.34	-1.29	15

3.3. Aboveground biomass mapping

The best model was applied across the landscape for mapping AGBt for the four selected study areas (Fig 8 a1-d1). At the landscape level and according to the given vegetation formation, the estimated mean and standard error of the AGBt estimates ranged from 21.28 to 99.35 Mg/ha and 9.03 to 25.39 Mg/ha, respectively (Table 5). Savanna and forest formations stored 48.09% (19.72 Mg/ha) and 78.58% (78.07 Mg/ha) more AGBt than grassland within our study sites. The uncertainty associated with the AGBt estimated mean was higher in the grassland than in savanna or forest formations (Table 5). In terms of spatial coverage, savanna was the most predominant contributing vegetation formation in the four study sites, which encompassed 59.8% of the total area, followed by forests (30.7%) and grassland (9.5%).

The use of high spatial resolution data from both GatorEye UAV-RGB and PlanetScope imagery allows for the delineation of the spatial distribution of each Cerrado formation for the four selected study areas (Fig. 8). Two sites showed all three vegetation formations (Fig 8a2, and c2), whereas one site showed both savanna and forest formations (Figure 8d2) and one site only savanna (Fig 8c2). The resulting histograms show the proportions of AGBt for each study site and Cerrado formation (Fig 8 a3-d3).

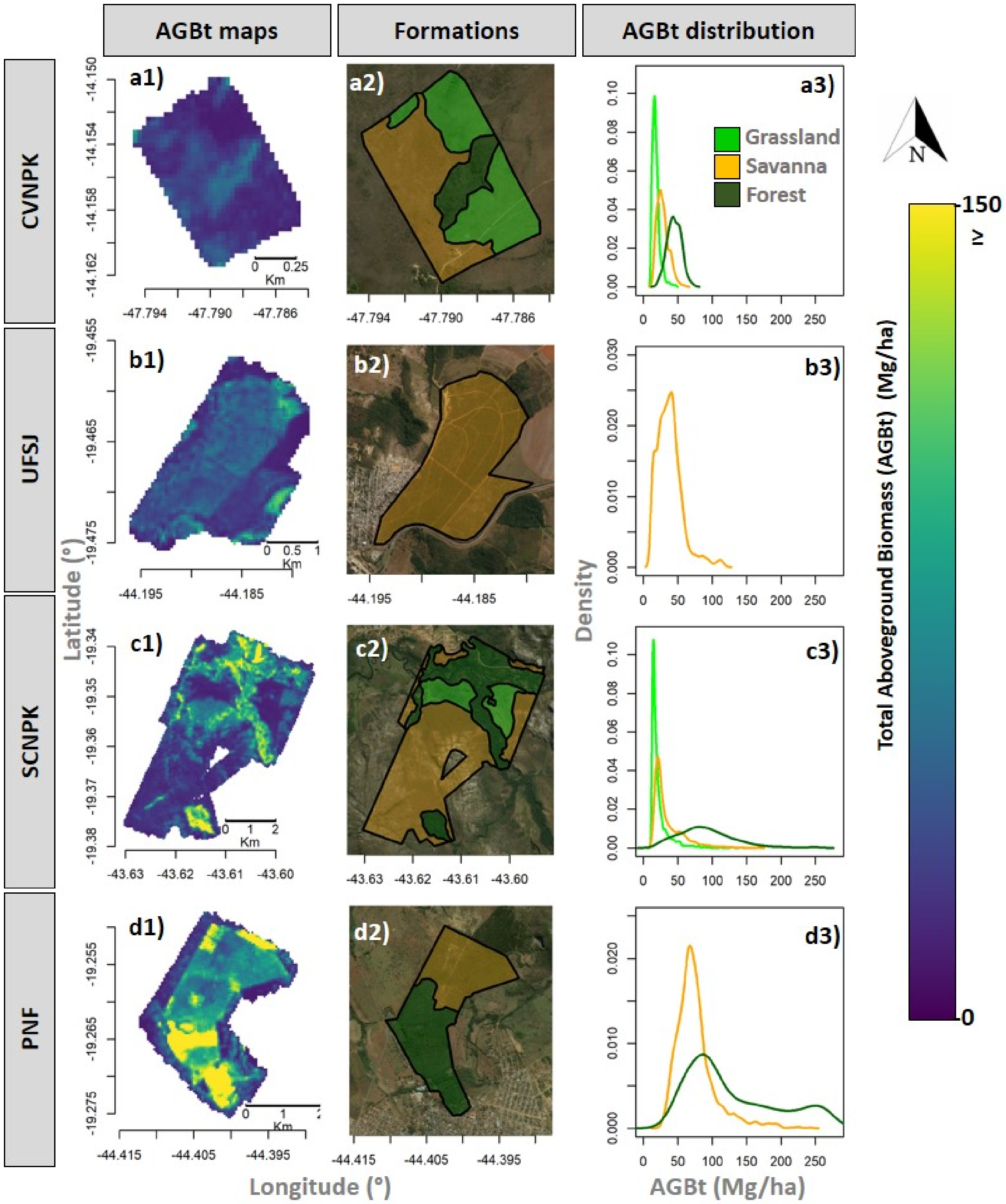

Figure 8. UAV-lidar derived maps of total aboveground biomass (AGBt) for the study sites a1-d1) with 30 m spatial resolution; Cerrado formation layers a2-d2) and distribution of the AGBt per vegetation formation in Cerrado.

Table 5. Summary of the total aboveground biomass (AGBt) and variance estimators at the landscape scale within the Cerrado formations. n = number of observations (mapped grid cells).

Cerrado Formation	$\widehat{E(\mu)}$	$V[\widehat{E(\mu)}]$	$\widehat{SE}$	$\widehat{SE}_{\%}$	n
Grassland	21.28	25.39	5.04	23.68	1,578
Savanna	41.00	9.03	3.00	7.33	10,044
Forest	99.35	15.64	3.95	3.98	5,160

4. Discussion

Cerrado is the second-largest source of carbon emissions in Brazil (Metzger et al. 2019), and hence accurate measurements of Cerrado AGBt are crucial for boosting vegetation carbon management, conservation, and restoration initiatives (Bispo et al., 2020). Our study demonstrates, for the first time, the potential of high-density UAV lidar sensors and the resultant 3-D point clouds to accurately capture the highly heterogeneous structure of tropical savanna in Brazil, which is characterized by the presence of various vegetation formations, including grassland, savanna, and forest. With this information, it was possible to model the AGBt, which also accounts for the role of small trees, shrubs, and surface vegetation biomass, as opposed to the majority of studies that have wholly focused on woody AGB of the canopy (e.g. Bispo et al., 2020; Zimbres et al., 2020). Our findings provide a glimpse of the large degree of errors associated with biomass estimations that can arise in cases where small trees, shrubs, and surface vegetation biomass pools are neglected and urges forest managers to adopt advanced measurement practices that consider AGBt.

4.1 Involving non-woody vegetation in lidar estimations of aboveground biomass

The lidar-assisted estimation of biomass from non-woody vegetation is largely neglected in the scientific literature, despite its large proportional importance to the global carbon cycles (van der Werf et al., 2010; Poulter et al., 2014; Pugh et al. 2019; Duvert et al., 2020; Lasslop et al., 2020). Although there are numerous studies regarding the use of lidar to estimate and monitor forest structure and AGB in a range of biomes and vegetation types (e.g. Clark et al., 2011; Hudak et al. 2012; Andersen et al., 2013; Asner and Mascaro, 2014; Silva et al., 2017), there is a scarcity of studies that include the full range of vegetation formations found in the Cerrado biome. Our results are not truly comparable to model performances obtained by other studies using lidar for biomass mapping in tropical savanna ecosystems, because the estimation is typically targeted solely to woody AGB (e.g. Bispo et al., 2020; Zimbres et al., 2020) as opposed to the AGBt estimation done in our study. For instance, Levick et al. (2019), using ALS for assessing habitat structure and woody aboveground carbon (AGC) response to altered fire regimes in tropical savanna in Australia, were able to calibrated models and map AGC to the entire experimental site with model performance resulting in a R^2 of 0.82 and RMSE of 7.35 Mg/ha, which implies about double in terms of AGB. Bispo et al. (2020) using also ALS derived top canopy height and cover for estimating only woody AGB showed good model performance with R^2 of 0.93 and RMSE of 6.74 Mg/ha (13.0%). Almeida et al. (2019) used the same GatorEye UAV-lidar system presented in this study, but in a tropical forest ecosystem, and were able map AGB across different forest successional stages with model performance in terms of R^2 of 0.80 and RMSE of24.9 Mg/ha (9.0%), respectively. The fact that the performance of our models was slightly worse than those presented by these authors can be explained by our approach to include non-woody vegetation in our estimation of AGBt, not just AGB stored in trees. For instance, Bispo et al. (2020) did not include data from grassland formations in their Cerrado gradient, which is the type of vegetation formation that typically yields higher errors in studies concurring to our results (Wang et al. 2017; Marselis et al., 2018; Zhang et al. 2018; Madsen et al., 2020). If shrubs and surface vegetation are not included in the sample, the resulting models cannot be extrapolated to map AGB toward grassland areas, which can be quite a representative proportion of the land in savanna ecosystems like Cerrado (Fig. 8). In turn, our results demonstrate that the estimation of AGBt is possible at a level of certainty comparable to estimating AGB from trees alone, which makes worth the extra effort in the sampling protocol compared to the gain obtained when including a proportionally relevant component of total vegetation biomass. Given the high importance of grassland estimation in savanna biomes (Simon et al., 2009), and their importance to global carbon balances (van der Werf et al., 2010; Poulter et al., 2014; Pugh et al. 2019; Duvert et al., 2020; Lasslop et al., 2020), it is crucial that further research lidar estimations of biomass includes non-woody vegetation formations in both the modelling to AGBt and sampling designs.

4.2 Convergence on metrics across sensors, platforms, and vegetation formations

We were able to identify the best UAV-lidar derived metrics to produce models that can accurately estimate the distribution of AGBt across the different vegetation formations, estimate total AGB at plot level, and produce maps at the landscape level for different regions of the Cerrado. The best model derived by exhaustive variable selection algorithm uses metrics that represent the top canopy height and cover (e.g. H98TH and COV), which concurs with typical results in other are common variables in models for AGB estimation in tropical ecosystems, including Cerrado (Levick et al. 2019; Bispo et al., 2020; Zimbres et al., 2020). For instance, Levick et al. 2019 were able to accurately map woody aboveground carbon (AGC) in tropical savanna in Australia using only lidar-derived canopy height and cover metrics. Bispo et al. (2020) used ALS for woody AGB mapping in Cerrado identified what models calibrated with top canopy height and cover resulted in better performances. Moreover, lidar-derived top canopy canopy height and cover metrics have shown to be stable at reduced pulse densities (Hansen et al., 2015; Silva et al., 2017), which enables the comparability of different surveys and thus the use of lidar time series (Bater et al., 2011; Hudak et al. 2012; Cao et al., 2016; Zhao et al., 2018; Hu et al. 2019). The scientific literature is clearly converging toward the use of these metrics, and thus they are already considered as standard ecosystem morphological traits to measure across multiple biomes and data sources (Valbuena et al., 2020). Our results show that these are also relevant in gradients including both forests and grassland ecosystems, which has great global implications (Simon et al., 2009). This convergence is enabling comparative meta-analyses across different types of 3-D remote sensing methods, to adequately assess different landscapes consistently (Valbuena et al., 2020). Thus, vegetation high (Asner and Mascaro, 2014) and cover (Tang et al., 2019) are as relevant to use for biomass estimation in grassland-dominated biomes as they are in forests. There have also been proved relationships between ecosystem vertical complexity and biomass stocks, using metrics related to entropy, variability or asymmetry (Zhang and Chen, 2015; Sullivan et al., 2017; Valbuena et al., 2017; Adnan et al. 2021).

4.3 Overcoming challenges in mapping total aboveground tropical savanna ecosystems

The complex physiognomy of ecosystems found in areas like Cerrado pases particular challenges to mapping biomass distributions using remote sensing. For this reason,there is only limited literature regarding the use of remote sensing to estimate AGBt, as compared to woody AGB estimation in savannas (Levick et al. 2019; Bispo et al., 2020; Zimbres et al., 2020). Accurate maps of AGBt can however help to identify the distributions of the different vegetation formations across the landscape, and their associated uncertainties. Our study thus serves as a benchmark for further data collection and could enable large scale availability of data regarding Cerrado biome structure. The accuracy of AGBt estimation, varied across different vegetation formations, with a greater uncertainty observed in grassland formations. This result may be associated with the smaller sample size for grassland and also the limitations of the UAV-lidar in capturing the 3-D structure for this formation. The high density of low-lying vegetation in the grassland, which lowers penetration of lidar pulses, can negatively impact the ability to differentiate vegetation returns from ground returns (Hopkinson et al. 2004; Streutker et al. 2006), introducing further errors and increasing the uncertainty. Such complications likely contribute to the apparent shortage of literature regarding the study of grassland vegetation with remote sensing (Hudak et al. 2016). Further research should focus more on involving the grassland areas with a stratified design (Adnan et al. 2021), since grassland areas area characterized by low AGBt values and they are typically largely neglected in the study design, and as a result the larger uncertainty associated with grassland data collection results in an underestimation of the overall AGBt.

4.4 Wider implications of our findings

The findings of this study, together with further research on this topic, can assist in the development of more accurate carbon monitoring and integrated fuel and fire management activities in Cerrado. For example, while developing maps of broad coverage, UAV-lidar can provide data for calibration and validation of satellite-based biomass maps, which are increasingly widely used owing to the proliferation of open-source platforms. Another critical and real-time applicability of UAV-lidar AGB maps are their contribution and potential for upscaling AGB maps and for validating satellite products, such as those from NASA's GEDI and ICESat-2 (Ice, Cloud, and land Elevation Satellite 2) missions (Silva et al., 2021). Consequently, UAV-lidar presents a convenient, relatively low-cost solution to collect data with an extremely high point density, thereby capturing and describing structural differences in the Cerrado. In tandem, these allow for the generation of highly accurate predictive models of total AGB for each Cerrado formation. The need for high-resolution assessments to calibrate and validate satellite-based biomass maps is crucial in the face of the enormous pressure that global changes are exerting on Cerrado. For instance, employing maps with higher uncertainty in grassland might limit or hinder the predictive capability of ongoing fire management strategies at Cerrado and warrant urgent attention in terms of their implications for practical applications. Currently, however, there is no better alternative in terms of speed and cost for large-scale estimation of AGBt in Cerrado, and so it may be the case that the greater quantities of UAV-lidar data and coverage compared to field measurements compensate for a slightly higher uncertainty for the predictions, especially over grassland formations.

4.5 Future directions

It is expensive and challenging to conduct fieldwork in the Brazilian Cerrado, and the existing field datasets still do not entirely represent the extent and complexity of the biome. This study has demonstrated UAV-lidar can successfully describe the Cerrado vegetation formations over large areas and has the potential to dramatically increase the size and accuracy of datasets that commonly misclassify Cerrado vegetation types on large scale satellites-derived AGB maps. The development of such AGB mapping techniques as those demonstrated in this study will have a strong impact on our ability to map and monitor AGB in the Cerrado biome, particularly with regards to the often-overlooked surface biomass. Nonetheless, the observed uncertainty in grassland should be investigated in-depth in future studies for improving AGB mapping accuracy, and for achieving this goal, we recommend testing the possibility of integrating TLS with UAV-lidar as well as evaluating the stand-alone accuracy observed via TLS techniques (Zimbres et al. 2020). Moreover, with increasing studies and field inventory expeditions in the grassland formations, we would be able the expand our data repository and evaluate how the number of sample study plots influences surface biomass estimation accuracies; this will also equip forest managers to determine the minimum amount of field plots required for estimating surface biomass in a satisfactory manner and help optimize data acquisition costs.

Future work that uses the workflows and outputs presented in this study to derive large scale, wall-to-wall AGBt maps have the potential to greatly contribute to improvements in carbon monitoring, and integrated fire and wildfire management. As the accuracy of remote sensing techniques improves, it may be the case that this study has provided a benchmark against which to show improvements in AGBt estimation for monitoring of carbon and wildfire management.

5. Conclusion

In this study, the use of UAV-lidar allowed us to accurately derive different vegetation metrics from 3-D point clouds to model and estimate total aboveground biomass at the landscape scale across the Cerrado formations at moderate-resolution. Our methodological approach may be upscaled to larger areas with success as it covers the main vegetation types of the biome, consisting of a gradient from grasslands to savannas and forests. Our modeling analysis identified the best lidar-derived metrics to be used to estimate total aboveground biomass, where the dominant vegetation height and canopy cover were the variables that showed the best model performance. The biomass map and framework presented in this paper can complement field assessments and train and validate other methods to estimate total aboveground biomass based on satellite data, such as GEDI. In this sense, users may potentially improve the spatial and temporal resolution of aboveground biomass monitoring in a region which plays a key role in the global carbon cycle and where the distribution of biomass is still unquantified. The study findings may support new decision support systems based on accurate monitoring of aboveground biomass aiming to inform and improve forest policy responses concerning issues of forest degradation, carbon emissions, and ecosystem function. Additionally, this assists in better understanding the climate-fire interactions and dynamic shifts in fire regimes arising from changes in biomass pools.

Acknowledgments

This project was supported by the Brazilian National Council for Scientific and Technological Development (CNPq) grant 442640/2018-8 (CNPq/Prevfogo-Ibama Nº 33/2018). D. R.A.A. was supported by the São Paulo Research Foundation (#2018/21338-3). A.C. was financed in part by MCTIC/CNPq Nº 28/2018 (#408785/2018-7; #438875/2018-4), CNPq Nº 09/2018 (#302891/2018-8). This research was financed in part by the Coordenação de Aperfeiçoamento de Pessoal de Nível Superior – Brasil (CAPES). M.E.F. is a CNPq Research Fellow (grant #315699/2020-5). We gratefully acknowledge the following undergraduate and graduate students involved in the field work campaign: Alberto A. Gontijo e Silva, Alexandre S. C. Filho, André Felipe C. Lima, Bernardo dos S. de Almeida, Carlos Magno M. de Oliveira, Gilberto do A. Pacheco; Gustavo R. Lattanzi, Iago Henrique F. da Silva, Irene M. Barbosa, Ivo S. Moreira, Jacson A. A. Machado, Jean Victor N. Paiva, Junia S. M. Macedo, Leandra Dietrich, Lídia A. de Aguiar, Matheus Gunther M. Soares, Nelson Amaral, Nivaldo R. J. Junior, Reginaldo Arthur G. Marcelino, Thiago Trajano. Moreover, we thank the park managers: Edward Elias Junior, Celso Lago-Paiva and Leandro Chagas from the Serra do Cipó National Park, Maria Carolina A. Camargos from the Chapada dos Veadeiros National Park and Renato Diniz Dumont from the Paraopeba National Forest. GatorEye data collection and processing by AMAZ and ENB was supported in part by the McIntire-Stennis program of the USDA, and the School of Forest Resources and Conservation and the Center for Latin America Studies at UFL.

Author Contributions:

M.B.T.C., C.A.S and R.V.L. designed the study. M.B.T.C., C.A.S, R.V.L., A.L.S., L.R.R.Y.G., V.A.C., D.R.A.A., A.H. and C.K.S. collected and processed the AGBt field data. E.N.B. and A.M.A.Z. collected and processed the UAV-lidar data. R.V., B.L.F., C.H.L.S.J., M.E.F., J.L., S.P.C.C., J.S. and A.C., C.H.A., contributed with the methodological framework, data processing analysis and write up. C.A.S., A.H., L.A., M.M., G.E.M., B.A.F.M., C.H., A.P.D.C., F.R., M.M., E.A.T.M., V.L. and M.E.F. contributed to the interpretation, quality control and revisions of the manuscript. All authors read and approved the final version of the manuscript.

Conflicts of Interest: The authors declare no conflict of interest.

References

Adnan, S., Maltamo, M., Packalen, P., Mehtätalo, L., Ammaturo, N., Valbuena. R. (2021). Determining maximum entropy in 3D remote sensing height distributions and using it to improve aboveground biomass modelling via stratification. (Submitted to Remote Sensing of Environment). Accessed Jan. 02 2021. Retrieved from https://dissertationesforestales.fi/pdf/article10467.pdf

Akaike, H. (1979). A Bayesian extension of the minimum AIC procedure of autoregressive model fitting. *Biometrika, 66*, (2), 237-242. https://doi.org/10.1093/biomet/66.2.237.

Almeida, DRA., Broadbent, EN., Zambrano, A. M. A., Wilkinson, BE., Ferreira, ME., Chazdon, R., Melia, P., Gorgense, EB., Silva, CA., Starkg, SC., Valbuena, R., Papa, DA., Brancalion, PHS. (2019). Monitoring the structure of forest restoration plantations with a drone-lidar system. *International Journal of Applied Earth Observation and Geoinformation*, *79*, 192-198. https://doi.org/10.1016/j.jag.2019.03.014

Almeida, DRA., Almeyda Zambrano, AM., Broadbent, EN., Wendt, AL., Foster, P., Wilkinson, B. E., Salk, C., Papa, DA., Stark, SC., Valbuena, R., Gorgens, E. B., Silva, C. A., Brancalion, PHS., Fagan, M., Meli, P., Chazdon, R. (2020). Detecting successional changes in tropical forest structure using GatorEye drone-borne lidar. *Biotropica*, *52 (6)*, 1156-1168. https://doi.org/10.1111/btp.12814

Alvarado, ST., Fornazari, T., Cóstola, A., Morellato, LPC., Silva, TSF. (2017). Drivers of fire occurrence in a mountainous Brazilian cerrado savanna: Tracking long-term fire regimes using remote sensing. *Ecological Indicators, 78 (1)*, 270-281. https://doi.org/10.1016/j.ecolind.2017.02.037

Alvares, CA., Stape, JL., Sentelhas, PC., De Moraes Gonçalves, JL., Sparovek, G. (2013) Köppen's climate classification map for Brazil. *Meteorologische Zeitschrift, 22 (6)*, 711-728.

Andersen, H., Reutebuch, S. E., Mcgaughey, R. J., Oliveira, MVN., Keller, M. (2013). Monitoring selective logging in western Amazonia with repeat lidar flights. *Remote Sensing of Environment, 151*, 157-165. https://doi.org/10.1016/j.rse.2013.08.049

Anderson, KE., Glenn, NF., Spaete, LP., Shinneman, DJ., Pilliod, DS., Arkle, RS., Mcllroy, SK., Derryberry, DR. (2018). Estimating vegetation biomass and cover across large plots in shrub and grass dominated drylands using terrestrial lidar and machine learning. *Ecological Indicators*, *84*, 793-802. https://doi.org/10.1016/j.ecolind.2017.09.034

Araújo, FM., Ferreira, LG., Arantes, AE. (2012). Distribution patterns of burned areas in the Brazilian Biomes: An analysis based on satellite data for the 2002-2010 period. *Remote Sensing*, *4* (7), 1929-1946. https://doi.org/10.3390/rs4071929

Asner, GP., Mascaro, J. (2014). Mapping tropical forest carbon: Calibrating plot estimates to a simple LiDAR metric. *Remote Sensing of Environment, 140*, 614-624. https://doi.org/10.1016/j.rse.2013.09.023

Balduino, APDC., Souza, ALD., Meira Neto, JAA., Silva, AFD., Silva Júnior, MCD. (2005). Phytosociological composition and floristic comparison of cerrado of Paraopeba flora-MG. *Revista Árvore, 29 (1)*, 25-34. https://doi.org/10.1590/S0100-67622005000100004

Bater, CW.; Wulder, MA.; Coops, NC.; Nelson, RF.; Hilker, T.; Naesset, E. (2011). Stability of sample-based scanning-lidar-derived vegetation metrics for forest monitoring. *IEEE Transactions on Geoscience and Remote Sensing, 49 (6)*, 2385-2392. https://doi.org/10.1109 / TGRS.2010.2099232

Benites, VM., Caiafa AN., Mendonça, ES., Schaefer CEGR., Ker, JC. (2003). Solos e vegetação nos Complexos Rupestres de Altitude da Mantiqueira e do Espinhaço. *Floresta e Ambiente, 10 (1)*, 76-85.

Bispo, PC., Rodríguez-Veiga, P., Zimbres, B., Do Couto De Miranda, S., Cezare, CHG., Fleming, S., Badalcchino, F., Louis, V., Rains, D., Garcia, M., Espirito Santo, MFDB., Roitman, I., Pacheco-Pascagaza, AM., Gou, Y., Roberts, J. Barret, K., Ferreira, LG., Shimbo, JZ., Alencar, A., Bustamanete, M., Woodhouse, LH., Sano, EE., Ometto, JP., Tansey, K., Balzter, H. (2020). Woody aboveground biomass mapping of the brazilian savanna with a multi-sensor and machine learning approach. *Remote Sensing, 12 (17)*, 2685. https://doi.org/10.3390/rs12172685

Bonanomi, J., Tortato, F. R., Raphael de Souza, R. G., Penha, J. M., Bueno, A. S., Peres, C. A. (2019). Protecting forests at the expense of native grasslands: Land-use policy encourages open-habitat loss in the Brazilian cerrado biome. *Perspectives in ecology and conservation*, 17(1), 26-31. https://doi.org/10.1016/j.pecon.2018.12.002

Breusch, TS., Pagan, ARA. (1979). Simple Test for Heteroscedasticity and Random Coefficient Variation. *Econometrica: Journal of the Econometric Society, 47 (1)*, 1287-1294. https://doi.org/10.2307/1911963

Broadbent, EN., Zambrano, AMA., Omans, G., Adler, A., Alonso, P., Naylor, D., Chenevert, G., Murtha, T., Vogel, J., Almeida, DRA., Dalla Corte, AP., Silva, CA., Prata, GA., Merrick, T., D'Oliveira, MVN., Detto, M., Ferreira, MP., Wilkinson, BE., Ferreira, ME., Muller-Landau, HC. (2020). In prep. The GatorEye Unmanned Flying Laboratory: sensor fusion for

4D ecological analysis through custom hardware and algorithm integration, accessed Set. 10 2020. Retrieved from http://www.gatoreye.org

Cao, L., Coops, NC., Innes, JL., Sheppard, SR., Fu, L., Ruan, H., She, G. (2016) Estimation of forest biomass dynamics in subtropical forests using multi-temporal airborne LiDAR data. *Remote Sensing of Environment, 178 (1)*, 158–171. https://doi.org/10.1016/j.rse.2016.03.012

Chave, J., Réjou-Méchain, M., Búrquez, A., Chidumayo, E., Colgan MS., Delitti, WBC., Duque, A., Eid, T., Fearnside, PM., Goodman, RC., Henry, M., Martínez-Yrízar, A., Mugasha, WA., Muller-Landau, HC., Mencuccini, M., Nelson, BW., Ngomanda, A., Nogueira, EM., Ortiz-Malavassi, E., Pélissier, R., Ploton, P., Ryan, CM., Saldarriaga, J. G., Vieilledent, G. (2014). Improved allometric models to estimate the aboveground biomass of tropical trees. *Global Change Biology*, *20 (10),* 3177–3190. https://doi.org/10.1111/gcb.12629

Clark, ML., Roberts, DA., Ewel, JJ., Clark, DB. (2011). Remote Sensing of Environment Estimation of tropical rain forest aboveground biomass with small-footprint lidar and hyperspectral sensors. Remote Sensing of Environment*, 115 (11)*, 2931–2942. https://doi.org/10.1016/j.rse.2010.08.029

Dalla Corte, AP., Souza, D. V., Rex, FE., Sanquetta, CR., Mohan, M., Silva, CA., Zambrano, AMA, Prata, G., Almeida, DRA., Trautenmuller, JW., Klauberg, C., Mpraes, A., Sanquetta, MN., Wilkinson, B., Broadbent, EN. (2020). Forest inventory with high-density UAV-Lidar: Machine learning approaches for predicting individual tree attributes. *Computers and Electronics in Agriculture*, *179 (1),* 105815. https://doi.org/10.1016/j.compag.2020.105815

Dass, P., Houlton, BZ., Wang, Y., Warlind, D. (2018). Grasslands may be more reliable carbon sinks than forests in California. *Environmental Research Letters*, *13* (7), 074027. https://doi.org/10.1088/1748-9326/aacb39

Drake, JB., Dubayah, RO., Clark, DB., Knox, RG., Blair, JB., Hofton, MA., Prince, S. (2002). Estimation of tropical forest structural characteristics using large-footprint coping. *Remote Sensing of Environment, 79 (2-3)*, 305-319. https://doi.org/10.1016/S0034-4257(01)00281-4

Dubayah, R., Blair, JB., Goetz, S., Fatoyinbo, L., Hansen, M., Healey, S., Hotfon, M., Hurtt, G., Kellner, J., Luthcke, S., Armston, J., Tang, H., Duncanson, L., Hancock, S., Jantz, P., Marselis, S., Patterson, PL., Wenlu, Q., Silva, C. (2020). The Global Ecosystem Dynamics Investigation: High-resolution laser ranging of the Earth's forests and topography. *Science of Remote Sensing*, *1*, 100002. https://doi.org/10.1016/j.srs.2020.100002

Durigan, G., Pilon, NAL., Abreu, RCR., Hoffmann, WA., Martins, M., Fiorillo, BF., Antunes, AZ., Carmignotto, AP., Maravalhas, JB., Vieira. J., Vasconcelos, HL. (2020). No Net Loss of Species Diversity After Prescribed Fires in the Brazilian Savanna. *Frontiers in Forests and Global Change, 3 (13)*, 1-15. https://doi.org/10.3389/ffgc.2020.00013

Durigan, G., Ratter, JA. (2016). The need for a consistent fire policy for Cerrado conservation. *Journal of Applied Ecology*, *53 (1)*, 11-15. https://doi.org/10.1111/1365-2664.12559

Duvert, C., Hutley, LB, Beringer, J., Bird, MI, Birkel, C., Maher, DT, Northwood, M., Rudge, M., Setterfield, SA., Wynn, JG (2020). Balanço líquido de carbono da paisagem de uma savana tropical: importância relativa do fogo e da exportação aquática na compensação da produção terrestre. *Global Change Biology*, *26* (10), 5899-5913. https://doi.org/10.1111/gcb.15287

D'Oliveira, MVN., Broadbent, EN., Oliveira, LC., Almeida, DRA., Papa, DA., Ferreira, ME., Zambrano, AMA., Silva, CA., Avino, FS., Prata, GA., Mello, RA., Figueiredo, EO., Jorge, LAC., Junior, L., Albuquerque, RW., Brancalion, PHS., Wilkinson, B., Oliveira-da-Costa, M. (2020). Aboveground Biomass Estimation in Amazonian Tropical Forests: a Comparison of Aircraft- and GatorEye UAV-borne LiDAR Data in the Chico Mendes Extractive Reserve in Acre, Brazil. *Remote Sensing, 12 (11)*, 1754. https://doi.org/10.3390/rs12111754

Felfili, J. M. (2007). Biogeografia do Bioma Cerrado: vegetação e solos da Chapada dos Veadeiros. (1 ª ed.). UnB: Finatec.

Ferreira, V., Mateus, L., Aguiar, J. (2012) Site recording using automatic image based three dimensional reconstruction techniques. *Proceedings of the International Conference on Computer Applications & Quantitative Methods in Archaeology,* CAA, 26–30.

Flores, BM., de Sá Dechoum, M., Schmidt, IB., Hirota, M., Abrahão, A., Verona, L., ... & Pamplona, MB. (2020). Tropical riparian forests in danger from large savanna wildfires. *Journal of Applied Ecology, 1 (1)*. https://doi.org/10.1111/1365-2664.13794

Franke, J., Barradas, ACS., Borges, MA., Menezes Costa, M., Dias, PA., Hoffmann, AA., Orozco Filho, JC., Melchiori, AE., Siegert, F. (2018). Fuel load mapping in the Brazilian Cerrado in support of integrated fire management. *Remote Sensing of Environment, 217 (1)*, 221–232. https://doi.org/10.1016/j.rse.2018.08.018

García, M., Riaño, D., Chuvieco, E., Danson, FM. (2010). Estimating biomass carbon stocks for a Mediterranean forest in central Spain using LiDAR height and intensity data. *Remote Sensing of Environment, 114 (4)*, 816-830. https://doi.org/10.1016/j.rse.2009.11.021

Goldbergs, G., Levick, SR., Lawes, M., Edwards, A. (2018). Hierarchical integration of individual tree and area-based approaches for savanna biomass uncertainty estimation from airborne LiDAR. *Remote sensing of environment, 205 (1)*, 141-150. https://doi.org/10.1016/j.rse.2017.11.010

Guimarães, JRC., Rios, PR. (2010). Martensite start temperature and the austenite grain-size. *Journal of materials science, 45 (4)*, 1074-1077. https://doi.org/10.1007/s10853-009-4044-0

Gwenzi, D., Lefsky, MA. (2016). Spatial modeling of Lidar-derived woody biomass estimates collected along transects in a heterogeneous savanna landscape. *IEEE Journal of Selected Topics in Applied Earth Observations and Remote Sensing, 10 (1)*, 372-384. https://doi.org/10.1109/JSTARS.2016.2582148

Harkel, JT., Bartholomeus, H., Kooistra, L. (2020). Biomass and crop height estimation of different crops using UAV-based LiDAR. *Remote Sensing, 12 (1)*, 17. https://doi.org/10.3390/rs12010017

Hansen, E.H.; Gobakken, T.; Næsset, E. Effects of Pulse Density on Digital Terrain Models and Canopy Metrics Using Airborne Laser Scanning in a Tropical Rainforest. Remote Sens. 2015, 7, 8453-8468.

Hernando, A., Velázquez, J., Valbuena, R., Legrand, M., García-Abril, A. (2017). Influence of the resolution of forest cover maps in evaluating fragmentation and connectivity to assess habitat conservation status. *Ecological Indicators, 79*, 295-302. https://doi.org/10.1016/j.ecolind.2017.04.031

Hirota, M., Holmgren, M., Van Nes, EH., Scheffer, M. (2011). Global resilience of tropical forest and savanna to critical transitions. *Science*, *334 (6053)*, 232-235. https://doi.org/10.1126 / science.1210657

Hu, T., Ma, Q., Su, Y., Battles, JJ., Collins, BM., Stephens, SL., Kelly, M., Guo, Q. (2019). A simple and integrated approach for fire severity assessment using bi-temporal airborne LiDAR data. *International Journal of Applied Earth Observation and Geoinformation, 78*, 25-38. https://doi.org/10.1016/j.jag.2019.01.007

Hudak, AT., Crookston, NL., Evans, JS., Falkowski, MJ., Smith, AM., Gessler, PE., Morgan, P. (2006). Regression modeling and mapping of coniferous forest basal area and tree density from discrete-return lidar and multispectral satellite data. *Canadian Journal of Remote Sensing, 32 (2)*, 126-138. https://doi.org/10.5589/m06-007

Hudak, AT., Strand, EK., Vierling, LA., Byrne, JC., Eitel, JUH., Martinuzzi, S., Falkowski, MJ. (2012). Quantifying aboveground forest carbon pools and fluxes from repeat LiDAR surveys. *Remote Sensing of Environment, 123 (1)*, 25–40. https://doi.org/10.1016/j.rse.2012.02.023

Hudak, AT., Dickinson, MB., Bright, BC., Kremens, RL., Loudermilk, EL., O'Brien, JJ., Ottmar, RD. (2016) Measurements relating fire radiative energy density and surface fuel consumption—RxCADRE 2011 and 2012. *International Journal of Wildland Fire, 25 (1)*, 25-37. https://doi.org/10.1071/WF14159.

Hudak, AT., Fekety, PA., Kane, VR., Kennedy, RE., Filippelli, SK., Falkowski, MJ., Tinkham, WT., Smith, AMS., Crookston, NL., Domke, GM. (2020). A carbon monitoring system for mapping regional, annual aboveground biomass across the northwestern USA. *Environmental Research Letters*, *15 (9)*, 095003. https://doi.org/10.1088/1748-9326/ab93f9.

Hopkinson, C., Chasmer, LE., Zsigovics, G., Creed, IF., Sitar, M., Treitz, P., Maher, RV. (2004). Errors in LiDAR ground elevation and wetland vegetation height estimates. *International Archives of Photogrammetry, Remote Sensing, and Spatial Information Sciences, 36 (8)*, 108-113.

Ibama. (1998). Parque Nacional da Chapada dos Veadeiros: Plano de manejo – Fase 3 (versão preliminar). (1ª ed.). Ibama.

Isenburg, M. (2020). LAStools—Efficient Tools for Lidar Processing. Accessed Dez. 16 2020. Retrieved from http://www.cs.unc.edu/~isenburg/lastools/

Lasslop, G., Hantson, S., Harrison, SP.,Bachelet, D., Burton, C., Forkel, M., Forrest, M., Li, F., Melton, JR., Yue, C., Archibald, S., Scheiter, S., Arneth, A., Hickler, T., Sitch, S. (2020). Global ecosystems and fire: Multi-model assessment of fire-induced tree-cover and carbon storage reduction. *Global Change Biology, 26,* 5027-5041.

Levick, SR., Shendryk, Y., Setterfield, S., Rossiter-Rachor, N. (2018). Evaluation of satellite remote sensing pathways for mapping and monitoring of gamba grass for the Savanna Fire Management Methodology. (1°Eds.), *Northern Australia Environmental Research Portal* (pp. 27) CSIRO and Charles Darwin University.

Levick, SR., Richards, AE., Cook, GD., Schatz, J., Guderle, M., Williams, RJ., Subedi, P., Trumbore, SE., Andersen, AN. (2019). Rapid response of habitat structure and above-ground carbon storage to altered fire regimes in tropical savanna. *Biogeosciences, 16 (7)*, 1493–1503. https://doi.org/10.5194/bg-16-1493-2019

Lindenmayer, DB., Wood, JT., Cunningham, RB., MacGregor, C., Crane, M., Michael, D., Montague-Drake, R., Brown, D., Muntz, R. Gill, AM. (2008). Testing hypotheses associated with bird responses to wildfire. *Ecological Applications, 18 (8)*, 1967-1983. https://doi.org/10.1890/07-1943.1

Luck, L., Hutley, LB., Calders, K., Levick, SR. (2020). Exploring the Variability of Tropical Savanna Tree Structural Allometry with Terrestrial Laser Scanning. *Remote Sensing, 12 (23)*, 3893. https://doi.org/10.3390/rs12233893

Lumley, T. (2020). Leaps: Regression Subset Selection. Thomas Lumley based on Fortran code by Alan Miller. R package version 3.1, accessed Dez. 16 2020. Retrieved from https://CRAN.R-project.org/package=leaps

Madsen, B., Treier, UA., Zlinszky, A, Lucieer, A., Normand, S. (2020). Detecting shrub encroachment in seminatural grasslands using UAS LiDAR. *Ecology and Evolution, 10 (11)*, 4876-4902. https://doi.org/10.1002/ece3.6240

Marselis, SM., Tang, H., Armston, JD., Calders, K., Labrière, N., Dubayah, R. (2018). Distinguishing vegetation types with airborne waveform lidar data in a tropical forest-savanna mosaic: A case study in Lopé National Park, Gabon. *Remote sensing of environment*, *216*, 626-634. https://doi.org/10.1016/j.rse.2018.07.023

Marselis, SM., Tang, H., Armston, J., Abernethy, K., Alonso, A., Barbier, N., Bissiengou, P., Jeffery, K., Kenfack, D., Labrière, N. (2019). Exploring the relation between remotely sensed vertical canopy structure and tree species diversity in Gabon. *Environmental Research Letters*, *14* (9), 094013. https://doi.org/10.1088/1748-9326/ab2dcd

Marselis, SM., Abernethy, K., Alonso, A., Armston, J., Baker, TR., Bastin, JF., Bogaert, J., Boyd, DS., Boeckx, P., Burslem, DFRP., Chazdon, R., Clark, DB., Coomes, D., Duncanson, L., Hancock, S., Hill, R., Hopkinson, C., Kearsley, E., Kellner, JR., Kenfack, D., Labrière, N., Lewis, SL., Minor, D., Memiaghe, H., Monteagudo, A., Nilus, R., O'Brien, M., Phillips, OL., Poulsen, J., Tang, H., Verbeeck, H., Dubayah, R. (2020). Evaluating the potential of full-waveform lidar for mapping pan-tropical tree species richness. *Global Ecology and Biogeography*, *29 (10)*, 1799-1816. https://doi.org/10.1111/geb.13158

Mohan, M., Silva CA., Klauberg, C., Jat, P., Catts, G., Cardil A., Hudak A., Dia, M. (2017). Individual Tree Detection from Unmanned Aerial Vehicle (UAV) Derived Canopy Height Model in an Open Canopy Mixed Conifer Forest. *Forests, 8 (9)*, 340. https://doi.org/10.3390/rs11101161

Metzger, JP., Bustamante, MM.; Ferreira, J., Fernandes, GW., Librán-Embid, F., Pillar, VD., Prist, PR., Rodrigues, RR.; Vieira, ICG., Overbeck, GE. (2019). Why Brazil needs its Legal Reserves. *Perspectives in Ecology and Conservation*, *17 (3)*, 91-103.https://doi.org/10.1016/j.pecon.2019.07.002

Naesset, E., Gobakken, T. (2008). Estimation of above-and below-ground biomass across regions of the boreal forest zone using airborne laser. *Remote Sensing of Environment, 112 (6)*, 3079-3090. https://doi.org/10.1016/j.rse.2008.03.004

Neri, AV., Schaefer, Ceg. R., Souza, AL., Ferreira-Junior, WG., Meira-Neto, JAA. (2013). Pedology and plant physiognomies in the cerrado, Brazil. *Anais da Academia Brasileira de Ciências*, *85 (1)*, 87-102. https://doi.org/10.1590/S0001-37652013000100007.

Oliveira-Filho, A. T., Ratter, J. (2002). Vegetation physiognomies and woody flora of the Cerrado biome. In Oliveira, PS., Marquis, TJ. (Eds.), *The Cerrados of Brazil: Ecology and natural history of a neotropical savanna* (pp. 91–120). Columbia University Press.

Ottmar, RD., Vihnanek, RE., Miranda, HS., Sata, MN., Andrade, SM. (2001). Stereo photo series for quantifying cerrado fuels in central Brazil. In: Volume I. (Eds.), *United States Department of Agriculture*, (pp. 1-87). Forest Service.

Prata, GA., Broadbent, E.N., de Almeida, DRA., St. Peter, J., Drake, J., Medley, P., Corte, APD., Vogel, J., Sharma, A., Silva, CA., Zambrano, AMA., Valbuena, R., Wilkinson, B. (2020). Single-Pass UAV-Borne GatorEye LiDAR Sampling as a Rapid Assessment Method for Surveying Forest Structure. *Remote Sensing*, *12 (24)*, 4111. https://doi.org/10.3390/rs12244111

Persson, HJ., Ståhl, G. (2020). Characterizing Uncertainty in Forest Remote Sensing Studies. *Remote Sensing*, *12 (3)*, 505. https://doi.org/10.3390/rs12030505

Pivello, VR. (2011). The use of fire in the cerrado and Amazonian rainforests of Brazil: Past and present. *ire Ecology*, *7 (1)*, 24-39. https://doi.org/10.4996/fireecology.0701024

Planet Team. (2017). Planet Application Program Interface: In Space for Life on Earth. San Francisco. Accessed Dez. 8 2020. Retrieved from https://api.planet.com

Porto, AC., Linares, JAH., Neto, GBS. (2011). Análise da estrutura e dinâmica da paisagem do Parque Nacional da Chapada dos Veadeiros. *Anais do Simpósio Brasileiro de Sensoriamento Remoto-SBSR*. INPE, 3057.

Poulter, B., Frank, D., Ciais, P., Myneni, RB., Andela, N., Bi, J., Broquet, G., Canadell, JG., Chevallier, F., Liu, YY., Running, S., Stich, S., Van der Wef, GR. (2014). Contribution of semi-arid ecosystems to interannual variability of the global carbon cycle. *Nature*, *509 (7502)*, 600-603. https://doi.org/10.1038/nature13376

Pugh, TA., Lindeskog, M., Smith, B., Poulter, B., Arneth, A., Haverd, V., Calle, L. (2019). Role of forest regrowth in global carbon sink dynamics. *Proceedings of the National Academy of Sciences*, *116 (10)*, 4382-4387. https://doi.org/10.1073/pnas.1810512116

Puliti, S., Saarela, S., Gobakken, T., Stahl, G., Næsset, E. (2018). Combining UAV and Sentinel-2 auxiliary data for forest growing stock volume estimation through hierarchical model-based inference. *Remote Sensing of Environment, 204*, 485-497. https://doi.org/10.1016/j.rse.2017.10.007

Qureshi, A., Badola, R., Hussain, SA. (2012). A review of protocols used for assessment of carbon stock in forested landscapes. *Environmental Science and Policy, 16 (1)*, 81–89, 2012. https://doi.org/10.1016/j.envsci.2011.11.001

Reichstein, M., Bahn, M., Ciais, P., Frank, D., Mahecha, MD, Seneviratne, SI, Zscheiscler, J., Cristã, C., Buchmann, N., Frank, DC., Papale, D., Ramming, A., Smith, P., Thonicke, K., Van Der Velde, M., Vicca, S., Walz, A., Wattenbach, M. (2013). Climate extremes and the carbon cycle. *Nature*, *500 (7462)*, 287-295. https://doi.org/10.1038/nature12350

Ribeiro, JF., Walter, BMT (2008). As principais fitofisionomias do bioma Cerrado. In: Sano, SM., Almeida, SP., Ribeiro, JF. (Eds.), *Cerrado: Ecologia e flora* (pp. 151-212). Embrapa Informação TeCColôgica.

Ribeiro, MC., Figueira, JEC. (2017). Uma abordagem histórica do fogo no Parque Nacional da Serra do Cipó, Minas Gerais–Brasil. *Biodiversidade Brasileira-BioBrasil, 1 (2)*, 212-227. https://doi.org/10.37002/biobrasil.v%25vi%25i.96

Ribeiro, SC., Fehrmann, L., Soares, CPB., Jacovine, LAG., Kleinn, C., Gaspar, RO. (2011). Above-and belowground biomass in a Brazilian Cerrado. *Forest Ecology and Management, 262 (3)*, 491–499. https://doi.org/10.1016/j.foreco.2011.04.017

Ribeiro, SC., Jacovine, LAG., Torres, CMME., Souza, AL. (2017) Influence of interspecific variation on tree carbon stock of a Brazilian Cerrado. *Revista Árvore, 41 (5)*, 1–11. https://doi.org/10.1590/1806-90882017000500006

Roitman, I., Bustamante, M. M., Haidar, R. F., Shimbo, J. Z., Abdala, G. C., Eiten, G., Lindoso, G. S. (2018). Optimizing biomass estimates of savanna woodland at different spatial scales in the Brazilian Cerrado: Re-evaluating allometric equations and environmental influences. *PloS one, 13 (8)*, 1-21. https://doi.org/10.1371/journal.pone.0196742

Saarela, S., Holm, S., Grafström, A., Schnell, S., NaesseT, E., Gregoire, TG., Nelson, RF., Stahl, G. (2016). Hierarchical utilizing three sources of information. *Annals of Forest Science, 73 (4)*, 895–910. https://doi.org/10.1007/s13595-016-0590-1

Scaranello, MAS., Keller, M., Longo, M., Santos, MN., Leitold, V., Morton, DC., Pinagé, ER., Espírito-Santo, FDB. (2019). Estimation of coarse dead wood stocks in intact and degraded forests in the Brazilian Amazon using airborne lidar. *Biogeosciences, 16 (17)*, 3457-3474. https://doi.org/10.5194/bg-16-3457-2019.

Schaefer, CE., Cândido, HG., Corrêa, GR., Nunes, JA., Arruda, DM. (2016). Soils associated with rupestrian grasslands. In: Fernandes, G.W. (Ed.), Ecology and Conservation of Mountaintop Grasslands in Brazil. Springer, Switzerland, pp. 55–69. http://dx.doi.org/10.1007/978-3-319-29808-53.

Shapiro, SS.; Wilk, MB. (1965). An Analysis of Variance Test for Normality (Complete Samples). *Biometrika, 52 (3,4)*, 591. https://doi.org/10.2307/2333709

Shendryk, Y., Sofonia, J., Garrard, R., Rist, Y., Skocaj, D., Thorburn, P. (2020). Fine-scale prediction of biomass and leaf nitrogen content in sugarcane using UAV LiDAR and multispectral imaging. *International Journal of Applied Earth Observation and Geoinformation, 92, (1)*, 102177. https://doi.org/10.1016/j.jag.2020.102177

Silva, JMC., Bates, J. M. (2002). Biogeographic patterns and conservation in the South American Cerrado: a tropical savanna hotspot: the Cerrado, which includes both forest and savanna habitats, is the second largest South American biome, and among the most threatened on the continent. *BioScience*, *52 (3)*, 225-234. https://doi.org/10.1641/0006-3568(2002)052[0225:BPACIT]2.0.CO;2

Silva, SR., Silva, AP., Munhoz, CB., Silva Jr, M. C., Medeiros, MB. (2001). Guia de plantas do Cerrado utilizadas na Chapada dos Veadeiros. (1ª ed.). WWF–Brasil.

Silva, CA., Klauberg, C., Carvalho, SPC. E, Hudak, AT., Rodriguez, LCE. (2014). Mapping aboveground carbon stocks using LiDAR data in Eucalyptus spp. plantations in the state of Sao Paulo, Brazil. *Scientia Forestalis, 42 (104)*, 591–604.

Silva, CA., Klauberg, C.; Hudak, AT., Vierling, L.A., Jaafar, WSWM., Mohan, M., Garcia, M., Ferraz, A., Cardil, A., Saatchi, S. (2017). Predicting Stem Total and Assortment Volumes in an Industrial *Pinus taeda* L. Forest Plantation Using Airborne Laser Scanning Data and Random Forest. *Forests, 8 (7)*, 254. https://doi.org/10.3390/f8070254

Silva, CA., Saatchi, S., Garcia, M., Labriere, N., Klauberg, C., Ferraz, A., Meyer, V., Jeffery, KJ., Abernethy, K., White, L., Zhao, K., Lewis, SL., Hudak, AT. (2018). Comparison of small- and large-footprint lidar characterization of tropical forest aboveground structure and biomass: A case study from Central Gabon. *IEEE Journal of Selected Topics in Applied Earth Observations and Remote Sensing*, *11 (10)*, 3512-3526. https://doi.org/10.1109/JSTARS.2018.2816962

Silva, CA., Duncanson, L., Hancock, S., Neuenschwander, A., Thomas, N., Hofton, M., Fatoyinbo, L., Simard, M., Marshak, CZ., Armston, J., Lutchke, S., Dubayah, R. (2021) Fusing simulated GEDI, ICESat-2 and NISAR data for regional aboveground biomass mapping. *Remote Sensing of Environment*, *253*, 112234. https://doi.org/10.1016/j.rse.2020.112234

Silva, VS., Silva, CA., Mohan, M., Cardil, A., Rex, FE., Loureiro, GH., Almeida, DRA., Broadbent, EN., Gorgens, EB., Dalla Corte, AP., Silva, EA., Valbuena, R., Klauberg, C. (2020). Combined Impact of Sample Size and Modeling Approaches for Predicting Stem Volume in Eucalyptus spp. Forest Plantations Using Field and LiDAR Data. *Remote Sensing*, *12 (9)*, 1438.

Simon, MF., Grether, R., de Queiroz, LP., Skema, C., Pennington, RT., Hughes, CE. (2009). Recent assembly of the Cerrado, a neotropical plant diversity hotspot, by in situ evolution of adaptations to fire. *Proceedings of the National Academy of Sciences*, *106(48),* 20359-20364. https://doi.org/10.1073/pnas.0903410106

Singh, RK., Kumar, P., Mukherjee, S., Suman, S.; Pandey, V., Srivastava, P. K. (2021). Application of geospatial technology in agricultural water management. In: *Agricultural Water Management,1 (1)*, 31-45. https://doi.org/10.1016/B978-0-12-812362-1.00003-5

Smith, RJ. (1993). Logarithmic transformation bias in allometry. *American Journal of Physical Anthropology, 90 (2)*, 215–228. https://doi.org/10.1002/ajpa.1330900208

Souza, CM., Júnior., Z. Shimbo, J., Rosa, MR., Parente, LL., A. Alencar, A., Rudorff, BFT., Hasenack, H., Matsumoto, M., G. Ferreira, L., Souza-Filho, PWM., de Oliveira, SW., Rocha, WF., Fonseca, A.V., Marques, CB., Diniz, CG., Costa, D., Monteiro, D., Rosa, ER., Vélez-Martin, E., Weber, EJ., Lenti, FEB., Paternost, FF., Pareyn, FGC., Siqueira, JV., Viera, JL., Neto, LCF., Saraiva, MM., Sales, MH., Salgado, MPG., Vasconcelos, R., Galano, S., Mesquita, VV., Azevedo, T. (2020). Reconstructing Three Decades of Land Use and Land Cover Changes in Brazilian Biomes with Landsat Archive and Earth Engine. *Remote Sensing, 12(17)*, 2735. https://doi.org/10.3390/rs12172735

Stahl, G., Saarela, S., Schnell, S., Holm, S., Breidenbach, J., Healey, SP., Patterson, PL., Magnussen, S., Naesset, E., Mcroberts, RE., Gregoire, TG. (2016). Use of models in large-area forest surveys: comparing model-assisted, model-based and hybrid estimation. *Forest Ecosystems, 3 (1)*, 1-11. https://doi.org/10.1186/s40663-016-0064-9

Staver AC, Archibald S, Levin SA. (2011). The global extent and determinants of savanna and forest as alternative biome states. *Science*, *334 (6053)*, 230-232. https://doi.org/10.1126/science.1210465

Streutker, DR., Glenn, N. F. (2006). LiDAR measurement of sagebrush steppe vegetation heights. *Remote Sensing of Environment*, *102* (1-2), 135-145. https://doi.org/10.1016/j.rse.2006.02.011

Sugiura, N. (1978). Further analysts of the data by akaike' s information criterion and the finite corrections. *Communications in Statistics - Theory and Methods, 7 (1)*, 13-26. https://doi.org/10.1080/03610927808827599

Sullivan, MJ., Talbot, J., Lewis, SL., Phillips, OL., Qie, L., Begne, SK., Miles, L. (2017). Diversity and carbon storage across the tropical forest biome. *Scientific Reports, 7 (1)*, 1-12. https://doi.org/10.1038/srep39102

Tang, H., Armston, J., Hancock, S., Marselis, S., Goetz, S., Dubayah, R. (2019). Characterizing global forest canopy cover distribution using spaceborne lidar. *Remote Sensing of Environment*, *231 (15)*, 111262. https://doi.org/10.1016/j.rse.2019.111262

Valbuena, R., Maltamo, M., Mehtätalo, L., Packalen, P. (2017). Key structural features of boreal forests may be detected directly using L-moments from airborne lidar data. *Remote Sensing of Environment*, *194 (1)*, 437-446. https://doi.org/10.1016/j.rse.2016.10.024

Valbuena, R., O'connor, B., Zellweger, F., Simonson, W., Vihervaara, P., Maltamo, M., Silva, CA., Almeida, DRA., Danks, F., Morsdorf, F., Chirici, G., Lucas, R., Coomes, DA., Coops, NC. (2020). Standardizing ecosystem morphological traits from 3D information sources. *Trends in Ecology & Evolution*, *3 (8)*, 656-667. https://doi.org/10.1016/j.tree.2020.03.006

Van der Werf, GR., Randerson, JT., Giglio, L., Collatz, GJ., Mu, M., Kasibhatla, PS., Morton, D C, DeFries, RS., Jin, Y., Van Leeuwen, TT. (2010). Global fire emissions and the contribution of deforestation, savanna, forest, agricultural, and peat fires (1997-2009). *Atmospheric Chemistry and Physics*, *10 (23)*, 11707-11735. https://doi.org/10.5194/acp-10-11707-2010

Wang, C., Shu, Q., Wang, X., Guo, B., Liu, P., Li, Q. (2019). A random forest classifier based on pixel comparison features for urban LiDAR data. *ISPRS journal of photogrammetry and remote sensing, 148 (1)*, 75-86. https://doi.org/10.1016/j.isprsjprs.2018.12.009

Wang, D., Xin X., Shao, Q., Brolly, M., Zhu, Z., Chen J. (2017). Modeling Aboveground Biomass in Hulunber Grassland Ecosystem by Using Unmanned Aerial Vehicle Discrete Lidar. *Sensors, 17(1)*, 180. https:// doi:10.3390/s17010180

Wilcoxon, F. (1945). Individual comparisons of grouped data by ranking methods. *Journal of economic entomology*, *39 (2)*, 269-270. https://doi.org/10.1093/jee/39.2.269

Wilkinson, B., Lassiter, HA., Abd-Elrahman, A., Carthy, RR., Ifju, P., Broadbent, E., Grimes, N. (2019). Geometric targets for UAS lidar. *Remote Sensing, 11 (24)*, 3019. https://doi.org/10.3390/rs11243019.

Zanne, A. E., Lopez-Gonzalez, G., Coomes, D. A., Ilic, J., Jansen, S., Lewis, S. L., ... & Chave, J. (2009). Global wood density database. Dryad. Identifier: http://hdl.handle.net/10255/dryad.235.

Zhang, H., Sun, Y., Chang, L., Qin, Y., Chen, J., Qin, Y., ... & Wang, Y. (2018). Estimation of grassland canopy height and aboveground biomass at the quadrat scale using unmanned aerial vehicle. *Remote sensing*, *10 (6)*, 851. https://doi.org/10.3390/rs10060851

Zhao, K., Suarez, J. C., Garcia, M., Hu, T., Wang, C., Londo, A. (2018). Utility of multitemporal lidar for forest and carbon monitoring: Tree growth, biomass dynamics, and carbon flux. *Remote Sensing of Environment*, *204*, 883-897. https://doi.org/10.1016/j.rse.2017.09.007

Zhang, Y., Chen, H. Y. (2015). Individual size inequality links forest diversity and above-ground biomass. *Journal of Ecology*, *103 (5)*, 1245-1252. https://doi.org/10.1111/1365-2745.12425

Zimbres, B., Shimbo, J., Bustamante, M., Levick, S., Miranda, S., Roitman, I., Alencar, A. (2020). Savanna vegetation structure in the Brazilian Cerrado allows for the accurate estimation of aboveground biomass using terrestrial laser scanning. *Forest Ecology and Management, 458 (1)*, 117798. https://doi.org/10.1016/j.foreco.2019.117798